Chapter 9

Plug Upgrade Calorimeter

9.1 Overview

The Plug Upgrade Calorimeter is a major component of the overall CDF upgrade program. This new calorimeter covers the polar angle region from $37°$ to $3°$, $(1.1 < |\eta| < 3.6)$ replacing the existing gas calorimeters, whose time response would have poorly matched the operational conditions of Run II (where the time interval between bunch crossings may be as low as 132 nsec). The top half of one plug is shown in cross section in Fig. 9.1. There is an electromagnetic (EM) section with shower position detection, followed by a hadronic section. In both sections the active elements are scintillator tiles read out by wavelength shifting (WLS) fibers embedded in the scintillator. The WLS fibers are spliced to clear fibers, which carry the light out to photomultipliers tubes (PMT) located on the back plane of each endplug.

The transverse segmentation of the Plug Upgrade Calorimeter is given in Table 9.1 and shown in Fig. 9.2. The segmentation of the EM and hadron towers are the same. This particular segmentation optimizes $e^{\pm}$ identification in $b/\bar{b}$ jets: $b \rightarrow e + X$, the details are discussed in Section 9.2.

The EM calorimeter is a lead/scintillator sampling type, with unit layers composed of 4.5 mm lead and 4 mm scintillator. There are 23 layers in depth for a total thickness of about 21 X_0 (radiation lengths) at normal incidence. The detecting elements are arranged in a tower geometry pointing back towards the interaction region. The η and ϕ segmentation of the central calorimeter is maintained as far as possible. The energy resolution of the EM section is approximately $16\%/\sqrt{E}$ with a 1% constant term.

The scintillator tiles of the first layer of the EM section are made out of 10 mm thick scintillator and are read out by Multi-Anode Photo-multiplier tubes (MAPMT). They will act as a preshower detector. A

Tower	Tile ID	$\Delta\eta$	$\Delta\theta$	$\Delta\phi$
10	EM Only	1.10-1.20	33-37°	7.5°
11	17,18	1.20-1.32	30-33°	7.5°
12	15,16	1.32-1.41	27-30°	7.5°
13	13,14	1.41-1.52	25-27°	7.5°
14	11,12	1.52-1.64	22-25°	7.5°
15	9,10	1.64-1.78	19-22°	7.5°
16	7,8	1.78-1.93	16-19°	7.5°
17	5,6	1.93-2.11	14-16°	7.5°
18	4	2.11-2.33	11-14°	15°
19	3	2.33-2.61	8-11°	15°
20	2	2.61-3.00	6-8°	15°
21	1	3.00-3.64	3-6°	15°

Table 9.1: The nominal transverse tower segmentation of the upgraded end plug calorimeter. The tower numbering is an extension of the CHA/WHA scheme.

position detector is located at the depth of the EM shower maximum (approximately 6 X_0). This shower maximum detector is made of scintillator strips read out by WLS fibers; clear fibers carry the light to MAPMTs.

The hadron calorimeter is a 23 layer iron and scintillator sampling device with unit layers composed of 2 inch iron and 6 mm scintillator. The existing iron of the CDF endplugs is used in the new hadron calorimeter. Stainless steel disks are attached to the inner 10° cone to extend the coverage to 3°. Two additional stainless steel disks are added behind the electromagnetic section to increase the thickness of the hadron calorimeter. In this way the magnetic field in the tracking volume and the magnetic forces on the end plugs are unchanged.

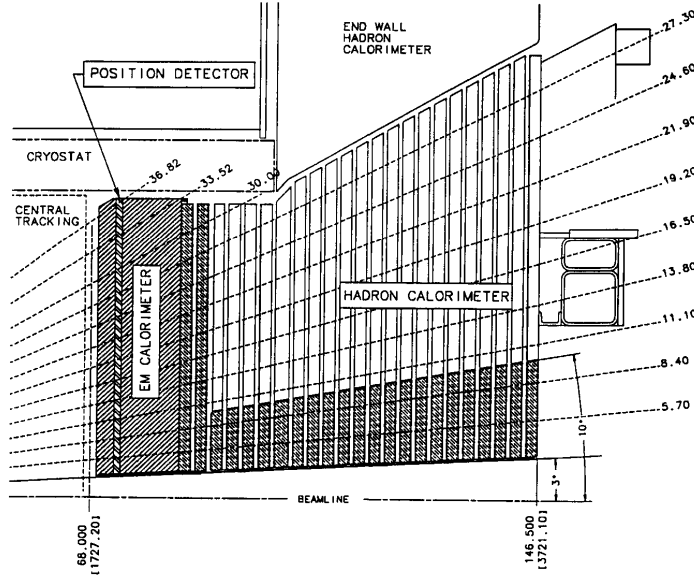The optical systems for the EM, hadron and shower

Figure 9.1: Cross section of upper part of new end plug calorimeter.

maximum detectors are very similar. The scintillator elements (tiles or strips) are cut from a large sheet of scintillator, and are assembled in triangularly shaped units called *megatiles*. The megatiles are installed into *pizza pans* that provide top and bottom optical covers and also protect the optical assembly. The pizza pans are installed into the EM (either scintillator tile layers for the calorimeters or scintillator strips for the shower maximum detector) and into the hadron calorimeters. Clear optical fiber cables connected to mass connectors on the outer edges of the pizza pans carry light to the rear face of the plugs. There the optical cables plug into *decoder boxes*, which change the grouping of fibers from pan-oriented to tower-oriented. The fiber groups coming from each tower are read out by PMTs connected to the decoder boxes.

A system of movable radioactive sources allows each tile (or strip) of the entire apparatus to be exposed to radiation during the construction phase, permitting us to measure the response of the device as we build it, and assuring us that we are maintaining quality control.

More general information on the Plug Upgrade project can be found in [1]. Table 9.2 summarizes the general characteristics of the Plug Upgrade Calorimeter.

Mechanical modifications to the existing plug iron and supports are discussed in section 9.3.2 of this

	EM	HAD
Segmentation	$\sim 8 \times 8 cm^2$	$\sim 24 \times 24 cm^2$
Total Channels	960	864
Thickness	21 X_0, 1 λ_0	7 λ_0
Density	$0.36\rho_{Pb}$	$0.75\rho_{Fe}$
Samples	22 +	23
	Preshower	
Active	4 mm Scint	6 mm Scint
Passive	4.5 mm Pb	2 inch Fe
Light Yield	≥ 3.5	≥ 2
(pe/MIP/tile)		
Resolution	$16\%/\sqrt{E} \oplus 1\%$	$80\%/\sqrt{E} \oplus 5\%$

Table 9.2: Overview of the Plug Upgrade Calorimeter. The EM (hadron) resolution is for a single electron (pion).

document, where the EM mechanical structure is also addressed. Section 9.10 describes early R&D studies on the engineering prototype. A detailed discussion of the complete optical system (excluding PMTs) is given in section 9.6. Sections 9.3, 9.5 and 9.4 describe design, manufacture, assembly, calibration, and quality control of the EM, hadron and shower maximum detectors respectively. Section 9.6.2 describes the PMT system, and the calibration and stability monitor systems are described in section 9.7 and 9.8. Finally, section 9.9 describes the Test Beam and Cosmic
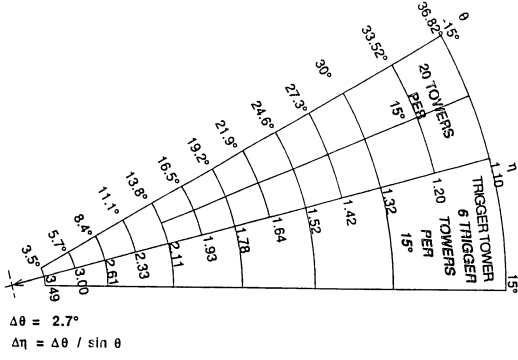
Figure 9.2: Transverse segmentation, showing physical and trigger towers in a 30° section.

Figure 9.3: Simulation result on the identification probability for electrons from $b \rightarrow e + X$ ($p_t^b > 5$ GeV).

Ray testing that will be performed on the assembled detector as part of the calibration program.

9.2 Specification of Transverse Segmentation

The transverse segmentation of the Plug Upgrade Calorimeter is given in Table 9.1 and shown in Fig. 9.2. It is the same for the EM and hadron compartments, and is the result of a Monte Carlo study on $e^{\pm}$ identification in $b/\bar{b}$ jets: $b \rightarrow e + X$. This is a good topology to use to tune the segmentation because the electron shower is in close proximity to a hadron jet. The Monte Carlo used ISAJET[2] to generate the $b/\bar{b}$ jets and CLEOMC2[3] to decay the resulting $b/\bar{b}$ hadrons. In this study, the $b/\bar{b}$ hadrons were forced to decay into electrons. One electron was required to be in the central region and the other in the plug. The electron tracks were marked and kept for later correlations with EM shower clusters.

A simplified detector simulation was used. It included the solenoidal magnetic field, the transverse EM and hadron shower shapes for transverse energy sharing among towers, and longitudinal energy sharing between the EM and hadron towers. Resolution smearing and detector cracks and transitions were not included. A cluster finder was used to find showers in the EM section. Electron identification cuts were applied to the EM cluster nearest to the electron track. The cuts required that the cluster energy (E_{em}) be consistent with the electron momentum (P_e) and that the energy in the hadron towers (E_{had}) directly behind the towers in the EM clus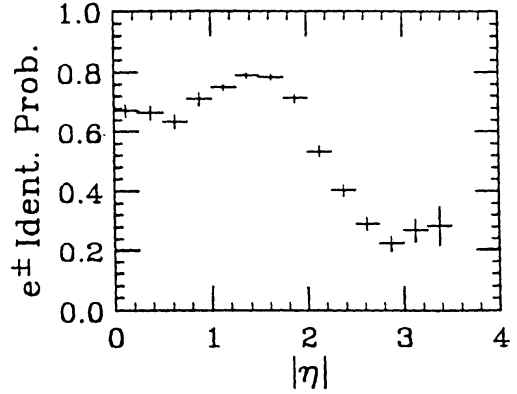ter be consistent with that for an electromagnetic shower: $E_{em}/P_e > 0.8$ and $E_{had}/E_{em} < 0.1$. Note that charged particle tracking capability down to the highest η is assumed. For the segmentation of Table 9.1, the probability that a $b \rightarrow e + X$ electron is isolated enough to be identified by tracking and calorimetry is shown in Fig. 9.3.

9.3 EM Calorimeter

9.3.1 Design Specification

The energy resolution of the EM calorimeter is given by:

$$\left(\frac{\sigma}{E}\right)^2 = \left(\frac{\sigma_1}{\sqrt{E}}\right)^2 + (\sigma_2)^2, \qquad (9.1)$$

where the first term $\sigma_1/\sqrt{E}$ comes from sampling fluctuations and the photostatistics of PMTs, and the second term σ_2 comes from the nonuniform response of the calorimeter. The sampling fluctuations from a 4.5 mm thick lead plate sandwiched between 0.5 mm thick stainless steel plates were estimated to be $14\%/\sqrt{E}$ using an EM shower simulation.

Our first design goal is that the energy resolution due to sampling should be less than $16\%/\sqrt{E}$. To achieve this, the light yield from a tile/fiber per MIP must be larger than 3 pe. The constant term contribution to the energy resolution is required to be less than 1%. To satisfy this requirement, the EM shower simulation showed that the transverse response within a tile/fiber assembly should have an r.m.s. less than 2.5%. The non–linearity of the calorimeter in the energy range between 10 GeV and 400 GeV should be less than 1%. To satisfy this re-

quirement, the variation of responses of tiles within a tower must be less than 10%.

The first layer of the EM calorimeter may be read out separately from the rest of the tiles in the same tower and can be used as a preshower detector, enhancing the physics capabilities of the EM calorimeter, particularly γ physics in the high η region. A careful analysis [13] has shown that to distinguish between γ and π^0 with good efficiency the light yield from the preshower layer at the PMT level must be at least 5 pe/MIP. This light yield will be achieved by increasing the thickness of the first layer tiles to 1 cm, and by using brighter BC-408 scintillator. The readout of the preshower detector will take place through MAPMT.

The design of the EM calorimeter is reviewed in Section 9.3.2 below. A full description of the design and construction of the EM calorimeter can be found in [14].

9.3.2 Mechanical Design

The mechanical structure of the EM calorimeter consists of 23 layers of lead absorber plates. The absorber plates, each 5.5 mm thick and approximately 2.77 m in diameter, are made of a calcium-tin-lead sheet (4.5 mm thick) sandwiched between 0.5 mm stainless steel sheets (Fig. 9.5) . Each lead layer is made of two 180° halves, while the steel sheets are laser cut into 45° sectors. Components are rotated such that edges do not overlap. The steel is epoxied to the lead over the whole surface area with a room temperature cure, while under vacuum.

At the inner diameter, 16 intermediate radial locations, and at 24 locations around the outer perimeter, stainless steel inserts are used in place of the lead and are spot welded to the steel sheets. These create *hard point* locations, which can be used to transfer the load of each sheet to the calorimeter support structure.

In 21 of the 23 layers, the absorber plates are held 8.8 mm apart by stainless steel spacers, allowing for the insertion of the standard EM section pizza pans. The structure thus allows for easy insertion and removal of the scintillator assemblies, and the scintillator assemblies are not loaded by the mechanical structure. This nominal dimension allows for the insertion of the 7 mm thick pans under all conditions, assuming a linear build-up of tolerances and deflections even when the calorimeter is stored horizontally, as in the Cosmic Ray test (see Sec. 9.9.2)

In the two slots corresponding to layers 1 and 5 the spacing is increased to 21 mm and 29.8 mm, respectively, to accommodate the preshower and shower maximum detectors. Layer 1 holds the preshower scintillator assemblies, while both the shower maximum detector and a standard EM pizza pan are placed in layer 5.

The 0.5 inch thick steel front plate of the calorimeter functions as an absorber layer (in terms of radiation lengths) while providing a good mechanical support. The entire structure, weighing about 13 tons (including the first iron layer, called -6 plate, to which the EM calorimeter is attached) is supported at the inside radius of the plates by a cone which transmits the load to the -6 plate, and from there to the hadron supports. In the installed position, the cone acts as a cantilever beam supporting the EM calorimeter, with the intermediate and outer spacers providing stability to the absorber plates as they are sandwiched between the 0.5 inch thick front plate and the 2 inch thick -6 plate. In the horizontal position, the cone and spacers allow for pan insertion and removal by limiting the deflections of each absorber sheet.

The EM calorimeter has the same diameter as the current PEM but is approximately 175 mm thinner. The resulting free space is used to re-establish a 25 mm stay clear zone between the front of the EM calorimeter and the Central Tracking region, and to add 2 more hadron layers behind the EM calorimeter.

9.3.3 Detector Description

The scintillator used for the calorimeter is Kuraray SCSN38 [15]. The WLS fiber and clear fiber are Kuraray multi-clad fibers with polystyrene for the core, polymethylmethacrylate (PMMA) for the inner cladding and fluorinated PMMA for the outer cladding. The 0.83 mm diameter Y11 WLS fibers are thermally spliced to clear fibers of the same diameter. The unspliced ends of the WLS fiber are mirrored by aluminum sputtering and coated with a cover of MgF_2.

The EM scintillator tiles are individually cut and arranged into 15° megatiles. Production starts with a scintillator plate roughly cut into a pair of 15° units. Fiber grooving and fine cutting are then performed. Next, the four edges of an individual tile are painted with a TiO_2 loaded O-de Coat (Nippon Paint). Extensive studies showed that it was best to place the tiles between two layers of white PET film (E65) to
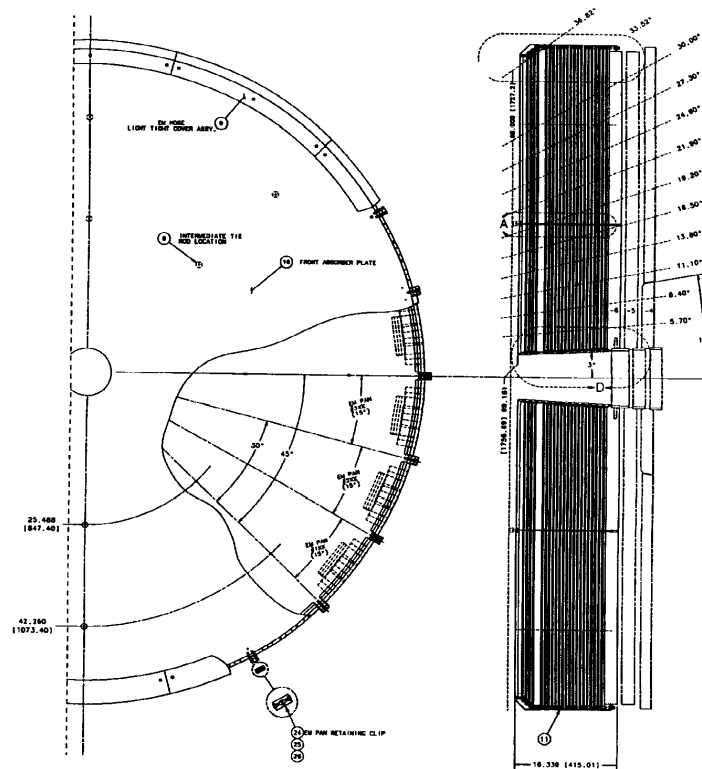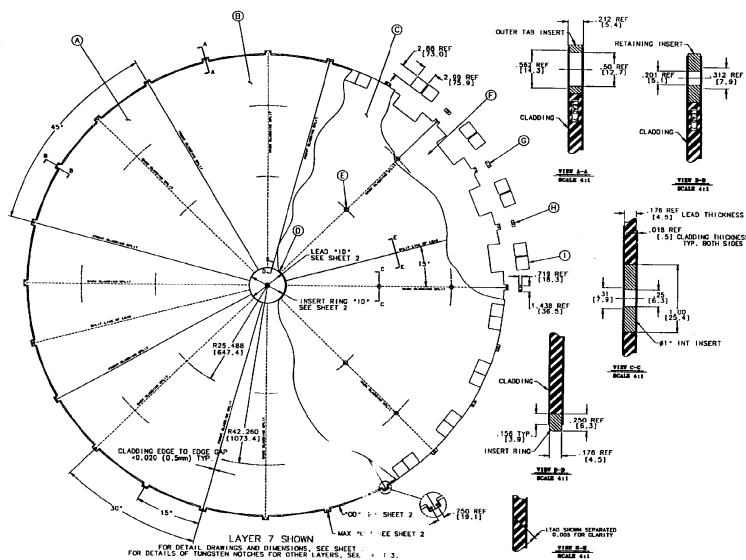
Figure 9.4: EM calorimeter mechanical structure.

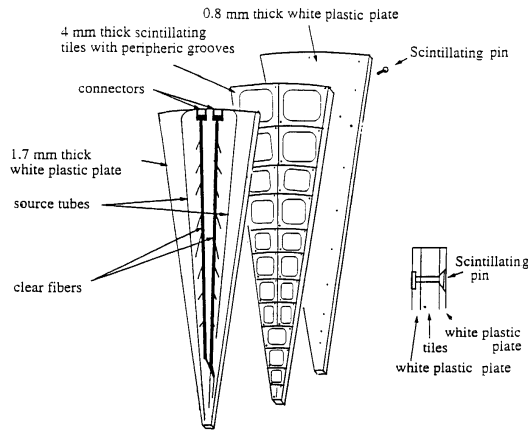Figure 9.5: Individual EM absorber plate.

Figure 9.6: Assembly scheme for an EM pizza pan.

Figure 9.7: Attenuation length distribution for 3 meter long WLS fibers.

provide good reflectivity on the tile surface and transverse uniformity of tile response. The assembly is therefore sandwiched between two layers of 1.7 mm and 0.8 mm thick white plastic sheets.

The tiles are accurately positioned with sets of scintillator pins (Fig. 9.6). The pins are 6.5 mm long and 3 mm in diameter. The scintillator pins were developed to minimize the non-uniformity of the response associated with the pins. Pin positions are staggered in subsequent layers. The scintillator pins were found to recover up to 75% of the light yield lost with conventional plastic pins.

9.3.4 EM Fiber Assembly Quality Control

Diameters of the fibers were checked. For the 0.9 mm clear fibers, the r.m.s. variation in diameter is 3.8 μm and the average diameters are close to 900 μm. No significant variation in average diameter between different production batches has been observed. These results satisfy our requirements of 900$\pm$20 μm. The WLS fibers were required to have diameters of 830$\pm$20 μm; fibers with diameters outside the specifications were rejected.

The WLS fibers were sampled and monitored for light yield and attenuation length. A 4 m long fiber piece was sampled out of every 50 m of WLS fiber. The 4 m fiber was divided into one 1 m long fiber and one 3 m long fiber, used for the light yield and attenuation length measurements respectively. The light intensity was measured by reading the current of a PMT (Hamamatsu H1161) while exciting the fiber from the side with an LED lamp at 5 cm length
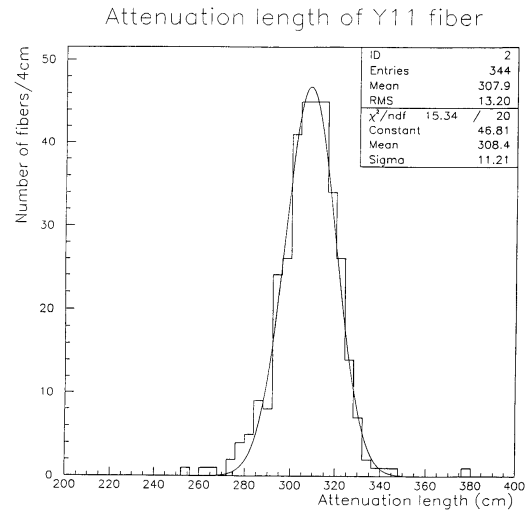
intervals. The attenuation length λ was obtained by fitting a plot of the light intensity vs. position to an exponential function.

The results of these measurements are shown in Figs. 9.7 and 9.8. The average attenuation length of WLS fibers is 308 cm, and the minimum attenuation length is 250 cm. The r.m.s. variation in attenuation length is 3.6%. The WLS fiber attenuation length was specified to be larger than 1.5 m with an r.m.s. variation from batch to batch below 15%.

For clear fibers, we sampled a pair of 15 m long fibers at the beginning and the end of each batch. The light from a halogen lamp was injected into one end of the clear fiber and the light intensity was measured at the other end by means of a spectrum analyzer at wavelengths of 500 and 670 nm. The fibers were then shortened by 3 m, the fiber ends were polished, and the transmission was measured again. Assuming exponential light attenuation, the attenuation length λ was obtained by the formula:

$$\lambda = -\frac{12 \ m}{\ln(I_1/I_2)} \qquad (9.2)$$

where I_1 and I_2 are the light intensity of the two measurements.

The average attenuation length of clear fibers at a wavelength of 500 nm is 9.3 m, and its r.m.s. variation is 11%. The average attenuation length of clear fibers at a wavelength of 670 nm is 21.4 m, and its r.m.s. variation is 21% . By an interpolation of the results at 500 nm and 670 nm, the attenuation length
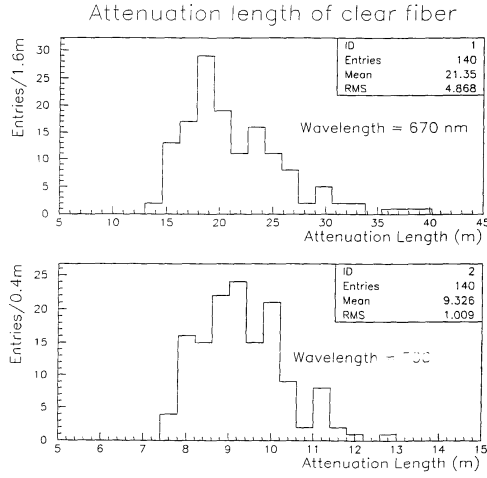
Figure 9.8: Attenuation length for clear fiber at two different wavelengths.

at 550 nm is estimated to be 12.9 m with an r.m.s. variation of 13.9%. For the clear fibers, the attenuation length was specified to be larger than 10 m and its r.m.s. variation less than 15% at a wavelength of 550 nm.

A full description of the quality control of the EM fiber assemblies can be found in [39].

9.3.5 EM Tile/Fiber Assembly Quality Control

The light yield of scintillator tiles mainly depends on plate thickness and dopant concentration. To ensure uniform response over a tile/fiber system, these two characteristics should be uniform. For samples of scintillator sheets produced by Kuraray, sheet thickness and light yield were measured. The average thickness is 4.0 mm and the r.m.s. thickness variation is 1.6%. The systematic uncertainty of the measurement of thickness variation is less than 0.01%.

The light yield of a block of scintillator sampled from a scintillator plate was required to be more than 130 pe/MIP, and its r.m.s. variation after correction for block thickness to be less than 2%. The light intensity of the sample block was reduced to 5% with a neutral density filter and air gaps in front of the PMT (Hamamatsu H1161). An EM shutter and a quartz glass in front of the PMT were used to keep the PMT high voltage on for the duration of the measurements and hence keep the gain of the PMT stable during the measurement. The light yields of all blocks were more than 140 pe. The results are shown
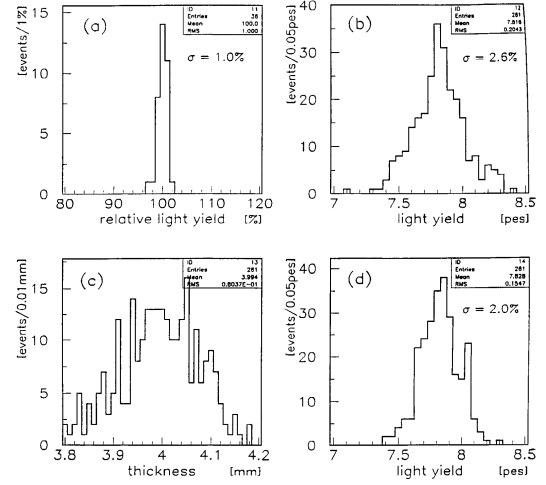

Figure 9.9: Light yield measurements on samples of Kuraray scintillator extracted from the production scintillator plates: (a) reproducibility of the measurement, (b) sample light yield, (c) sample thickness (d) sample light yield after thickness correction.

in Fig. 9.9. The r.m.s. variation of the thickness-corrected light yields was 1.7% after subtracting 1% systematic error. These results satisfy the requirements.

To investigate the final response of the tile, about 2% of tiles were sampled and their light yields for MIPs were measured using several standard fibers. The final requirement for the light yield is that the light yield must be at least 3 pe/MIP/tile. In previous studies, it was found that about 20% of the light was lost at the splice, about 10% of the remaining light was lost at the fiber connector, and about 40% of the light was lost in a 5 m clear fiber (the attenuation length of clear fibers is approximately 10 m). In total, approximately 60% of the light from a tile is lost before reaching the PMT.

In measurements of tile/fiber light yield after the tile fabrication, scintillator tiles and standard WLS fibers were used. The WLS fiber length was typically 60 cm, and the light from the WLS fiber was directly measured without clear fiber or fiber connectors. We required that the light yield be more than 12 pe/MIP in this measurement. The light yields from sample tiles were corrected using the light yields from reference tiles. We monitored the light yield of the reference tile before and after all the measurements. The r.m.s. variation of the light yield after subtracting the variations in WLS light yield and sample tile thickness was required to be less than 2%.

After the final assembly, a cosmic-ray test of all the 15° units (1144 units) as a final quality control procedure was done. 15 pans at a time were exposed to cosmic rays for a period of 24 hours. The reproducibility of the light yield measurement is approximately 3%. The quality requirements are

- light yield of the tile per MIP larger than 3.5 photo-electrons,

- light yield within $\pm 30\%$ with respect to the tower average,

- light leakage to adjacent tiles less than 3.5%.

The light yield r.m.s. for tiles of the same size measured by the cosmic ray setup for 880 units was 5.4%. The r.m.s. for tiles belonging to the same tower was measured to be 9.5%. A full description of the quality control of the EM Tile/Fiber Assemblies can be found in [39].

9.4 Shower Maximum Detector

9.4.1 Design Specification

The Plug Upgrade Calorimeter shower maximum detector (SMD) is a position sensitive detector placed at a depth of approximately 6 radiation lengths inside the EM calorimeter. It will cover a circular area 2.6 m in diameter at 1.8 m from the nominal interaction point at B0. Its purpose is twofold:

- measure the position of $e^{\pm}$ and γ showers

- help separate $e^{\pm}$ and γs from π^0.

The design of the SMD is constrained by the overall design of the plug calorimeter. For example, since the EM calorimeter is based on 15° azimuthal sectors, it is prudent to choose the SMD sector angle to be an integer multiple of 15°. Various position detector scenarios have been investigated in the past [20]. The technical solution finally chosen for the SMD consists of scintillator strips read out by WLS fibers. Test beam studies and Monte Carlo simulations [21] have shown that an output of 1 pe/MIP should be sufficient for the measurement of the position of high energy electrons with resolution of approximately 1 mm in a detector made of 5 mm wide strips.

Requirements imposed by physics issues have also been addressed. The segmentation scheme has been finalized after careful studies of π^0/γ separation, occupancy and resolution of ambiguities caused by multiple showers. Although not a design requirement, sensitivity to muons would be useful. Ability to detect minimum ionizing particles efficiently requires about 4 pe/MIP. Test beam studies and Monte Carlo simulations show that an r.m.s. response variation of 10% between detector channels does not significantly degrade position resolution or π^0/γ discrimination.

Since the detector will be read out by a MAPMT and presently available devices generally have channel to channel gain variations greater than 10%, we consider careful channel to channel calibration of this detector a crucial factor in its successful commissioning. Moreover, because of scintillator aging and potential radiation damage, it will be necessary to monitor the calibration during the course of operation. The calibration system employs a 5 mm ^{137}Cs wire source running almost perpendicular to the strips in the SMD plane. The current read out from each channel of the MAPMT provides the strip to strip calibration.

9.4.2 Detector Description

The active elements of the SMD are scintillator strips read out with WLS fibers. The WLS fibers are connected through optical connectors to clear fibers, which carry the light to the MAPMTs located at the rear of the plug.

The SMD is divided into eight 45° sectors, each covering the region from the beam pipe at 11 cm to an outer radius of 130 cm. Each sector contains two layers (called U and V) of 5 mm pitch scintillator strips. The U and V layers are held together by two 1/8" thick lexan covers, and inserted into the fifth sampling slot (behind $\approx$6 radiation lengths of material) within the EM calorimeter

The placement of the U and V strips in a 45° sector are shown in Fig. 9.10. The two scintillator layers U and V are aligned at +22.5° and −22.5° with respect to the radial dimension, to provide two-dimensional position measurement. Monte Carlo studies show that π^0 rejection increases with increasing U-V crossing angle, and that U-V angles greater than 30° are necessary for good rejection efficiency. This design employs a 45° crossing angle as the most reasonable choice, since larger angles would be difficult to implement mechanically.

Each U or V layer will be assembled with 400 scin-
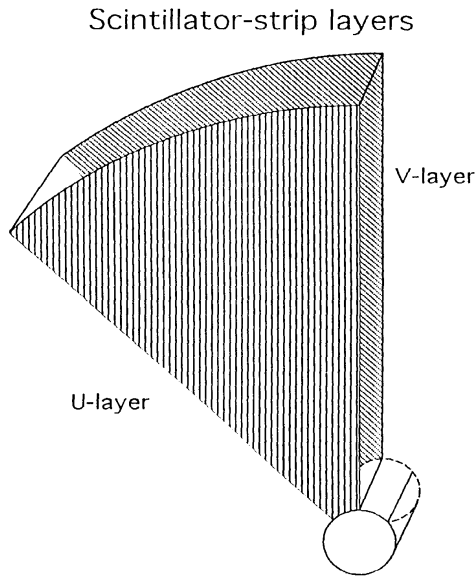
Scintillator-strip layers

Figure 9.10: Geometry of the SMD in a 45° sector

tillating strips aligned parallel to one edge or the other of the 45° sector. The scintillating strips are 5 mm wide by 6 mm thick and have variable length between 5 and 100 cm. A "ball groove" in each strip (0.89 mm in diameter) accepts a WLS fiber (0.83 mm in diameter) which guides the light to optical connectors mounted near the outer perimeter of the sector. The strips are wrapped like a tennis racket grip with reflective aluminum tape. Groups of 10 strips are taped together and subsequently treated as one unit, which we call a "megastrip". The megastrips are placed in the pizza pans using separators that keep the megastrips parallel to one side of the 45° sector.

The U and V scintillator strip layers are segmented into upper and lower parts, corresponding to η regions 1.13-2.60 and 2.60-3.50 respectively. The upper and lower strips are separated at a line that intersects the side of the panel at a radius of 28.2 cm, matching the EM calorimeter inter tile boundary. The main purpose of η segmentation is to reduce the occupancy of the strips expected from the underlying event. Although the occupancy expected in the lower η segment is approximately two to four times larger than that of the upper segment, further segmentation is impractical. In tests performed, we found that the light yield decreases as the strips become shorter. For efficient light collection, the strip length should not be smaller than 5 cm. For this reason, and also for the practical reason of avoiding very short strips, the

short strip corner of the lower sector is serviced by strips from the upper sector, while the short strips of the upper sector are eliminated.

Three megastrips will service the high-η region. The WLS fibers in these megastrips will be spliced to clear fibers routed underneath the scintillator strips of the low-η region, using the grooves milled in the lexan covers.

9.4.3 SMD Fiber Assembly Quality Control

The WLS fibers were prepared prior to the pizza pan assembly in a manner very similar to that described below for the hadron calorimeter. One end of each WLS fiber was polished, mirrored by aluminization, and protected by a thin coating of epoxy glue. The other end was cut to a specified length and inserted into a 10-fiber optical connector. The fiber ends were then glued in place in the connectors and polished. The WLS fibers from the scintillator strips from the lower part were first spliced to clear fibers.

The r.m.s. variation in transmission through the fibers and connector assemblies was around 2%. This value is in agreement with the observation made during the production of the hadron calorimeter (section 9.5) and the difference in quadrature between the two observed r.m.s. values is in good agreement with the values reported in Ref.[7] for the variation in the light transmission through a splice. We accepted all fiber/connector assemblies where the light yield was within 10% ($\pm 4\sigma$) of the average light yield for unspliced fibers and within 15% ($\pm 4\sigma$) of the average light yield for spliced fibers.

9.4.4 SMD Scintillator Strips and Megastrips Quality Control

Before turning to the production of the scintillator strips and megastrips, we measured the individual light yield of all the BC408 scintillator plates received from the vendor (Bicron). We used a ^{207}Bi source to determine the response of samples of scintillator to ~ 1 MeV electrons depositing all their energy in the scintillator All the plates for which the response was more than 10% away from the average response were rejected and sent back to the vendor for replacement.

All assembled pizza pans were scanned sending a wire with a 4 mCi ^{137}Cs source mounted on the tip through the source calibration tubes mounted on each pizza pan, and by scanning all the individual
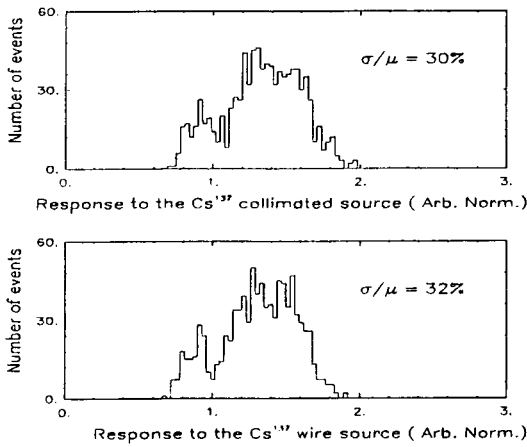
Figure 9.11: Response of the SMD fiber/strip assemblies to the collimated and wire-mounted ^{137}Cs sources.

Figure 9.12: Correlation (top) and ratio (bottom) between the responses to the collimated and wire-mounted sources.

strips with a collimated ^{137}Cs source. The strips were read out through a 64 channel MAPMT, the DC anode current of which was measured by a picoammeter. The individual channel read out test was repeated for all the strips in all the pans. The motivation for this test was to determine whether the calibration system (source tubes running on the outside of pizza pan and crossing the strips at an angle of 67.5°) would have ensured a strip to strip calibration uncertainty of 10% (or less).

Figure 9.11 shows the responses of the individual strips to the collimated and wire-mounted sources for a subset of strips where the crossing angle between the source tubes and the strips is constant. The variation in strip response is mainly due to the channel to channel response variation of the MAPMT which are exactly what we want to calibrate out with the wire source. Figure 9.12 (top) shows the correlation between the responses to the collimated and the wire sources. The correlation is outstanding, and the r.m.s. variation in the correlation is about 4% which is more than two times better than required.

Figure 9.12 (bottom) shows the ratio between the responses to the collimated and wire sources as a function of the strip number for the first 60 strips of the full set of shower maximum pizza pans. The higher response in the low numbered channels is due to the fact that the source tube crosses closer to the long axes of these fingers, and the source activity is about 5 mm long. We are presently working to understand all these marginal effects of the wire source system.
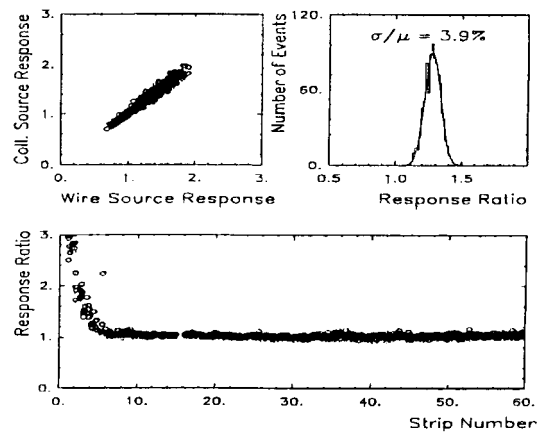
9.5 Hadron Calorimeter

9.5.1 Design Specification

The hadron calorimeter has been designed to attain the following performance: first, its $\eta - \phi$ segmentation should allow the topics such as b-physics, W, Z, and γ physics, and jet physics, to be investigated in an efficient and productive fashion. Second, it should have an energy resolution of $\sigma/E \sim (80 - 90)\%/\sqrt{E} \oplus 5\%$. This is dominated by the sampling fluctuations from 2" steel absorber plates rather than by PMT photostatistics and response variation. For such sampling, the sensitivity of the calorimeter to hadron showers is 0.1 GeV/MIP/tile and the intrinsic resolution is $\sim 80\%/\sqrt{E}$. Finally, the calorimeter should be able to identify muons via their dE/dx energy loss.

The engineering prototype and subsequent R&D indicate that the hadron calorimeter will attain the target energy resolution of $(80 - 90)\%/\sqrt{E} \oplus 5\%$. In terms of component performance, the 5% constant term requires that the r.m.s. variation of tile to tile light yield be better than 10% and that the r.m.s. of intra-tile transverse nonuniformity be less than 4% (assuming the nonuniformity is the same for all tiles in a projective tower). An overall tile to tile light output variation of 10% contributes only 3% to the constant term because the hadron shower is typically spread out over more than 10 layers longitudinally.
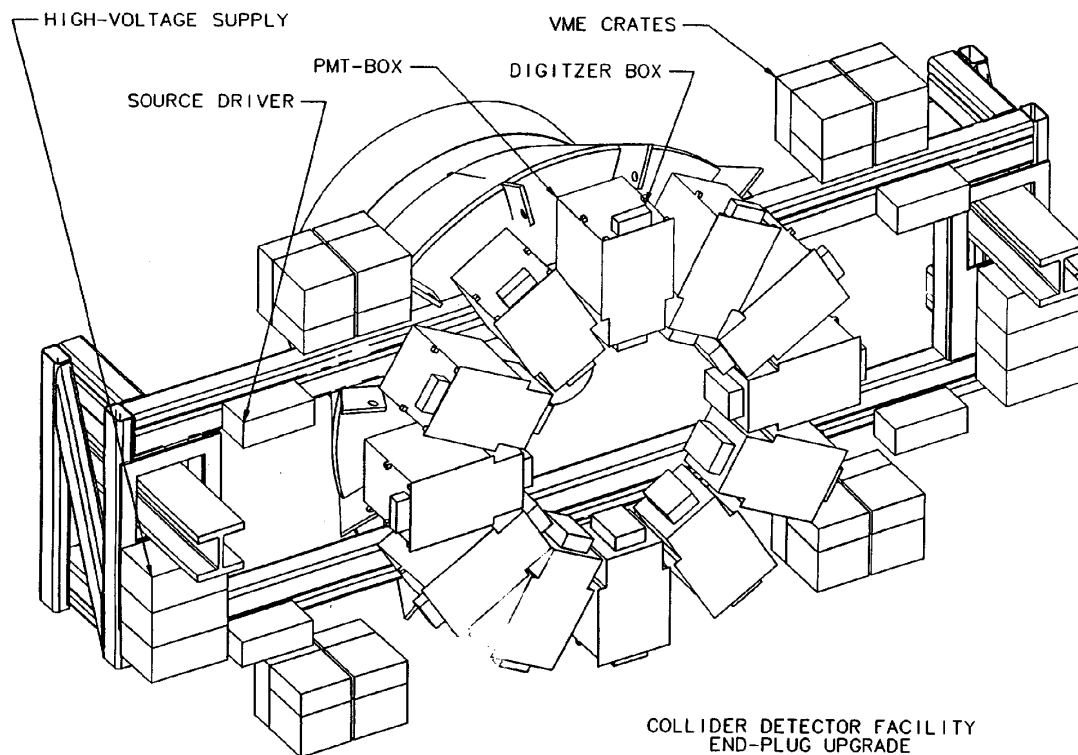
Figure 9.13: End plug calorimeter support structure.

9.5.2 Mechanical Design

9.5.2.1 Hadron Module

The steel structure of the existing hadron calorimeter will be reused, after two modifications: first, the addition of two two-inch thick stainless steel plates to the front of the calorimeter and the replacement of the existing -4 plate; second, the addition of stainless steel disks to each of the existing iron absorber to close the region around the beam line from $10°$ to $3°$ (Fig. 9.1).

The additional plates in front of the hadron detector will be supported in the same manner as the plates located in the cylindrical region of the existing hadron calorimeter, namely by cantilever beams which extend forward from the 0 plate every $30°$ around the perimeter of the device. Each of these additional plates will be attached to the calorimeter in the assembly hall, with the -6 plate arriving as the backplate of the EM calorimeter. The -4 plates will be replaced by spares from the original plugs. The carbon steel portion of the -4 plate will remain 1.75 inch thick, as in the current structure, to minimize change in the magnetic field.

After being stripped of the old calorimeter gas chambers, the existing plug steel will be rotated nose down, and the $10°$ to $3°$ stainless steel disks will then be welded to each of the existing hadron plates sequentially, front to back, in the calorimeter. The inner tie ribs which currently support the plates in the $10°$ region will be taken out; their function is served by rings joining the stainless steel inserts at their inner diameter. These rings will also serve to make the structure light tight in this region.

The additional steel adds about 7 tons to the weight of each end plug, and the center of gravity of each plug moves towards the interaction point. The design for the modifications to the hadron structure have passed the safety review.

9.5.2.2 Design and Analysis of the End Plug Support Structure

The EM and hadron modifications increase the weight of each end plug by approximately 13 tons, to 102 tons total, and move the center of gravity of

each plug towards the interaction point by 175 mm. However, the plugs will continue to be supported by the existing box beam structure after reinforcement in a few critical areas. The removal of several vertical plates on the rear of each plug will create additional area for PMT mounting and electronics, as shown in Fig. 9.13.

The original analysis of the support structure treated the detector in terms of two separate components: the calorimeter and the support structure. However, during assembly the rear plate of the hadron calorimeter was welded to the box beam supports, making the vertical plates redundant. Two of the original four plates have been removed from each plug, and with this upgrade we will remove the remaining two plates, as their function is served by the 2 inch thick hadron steel plate to which the beams are attached. Several 1 inch thick plates will be added to the box beams to increase the overall stiffness of the structure, limiting both the stresses and deflections.

An ANSYS model of the end plug structure has identified these areas of concern, and the new plates can be seen in Fig. 9.13. These plates will be added when the structure is rotated nose down for the addition of the hadron steel disk inserts. The I-beams on the central calorimeter which support the plug as it is rolled into place have also been included in the ANSYS analysis, and some reinforcement of these beams, or limitation of the total travel of the plugs, will have to be implemented.

9.5.3 Hadron Pizza Pan Assembly

In contrast to the EM sector, all 32 tiles within a 30^0 section are cut from a single piece of scintillator. A cross section of the pizza pan unit is shown in Fig. 9.14. The unit begins with a 0.063" thick aluminum bottom cover. Then comes the 6 mm thick SCSN38 scintillator megatile covered on both sides with 0.006" thick white reflective Tyvek [16] paper. The surfaces of the scintillator tiles are grooved to hold the WLS fibers.

Above the megatile is a 0.150" thick white plastic fiber routing sheet. The fibers rise out of the scintillator through a 0.125" × 1" slot in the white plastic into grooves on the top side of the white plastic. The grooves, 0.063" wide and 0.063" deep, route the fibers to an optical connector at the outside edge of the pan. Source calibration tubes, 0.050" O.D., are placed on the bottom of the white plastic. There are four cal-
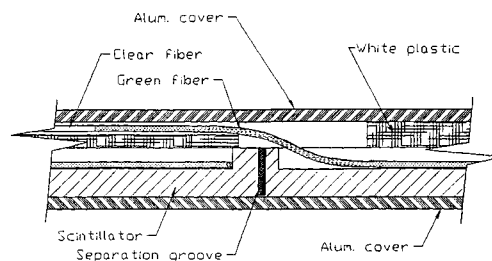

Figure 9.14: Hadron pizza pan cross section.

ibration tubes per megatile and each tile is crossed by one tube. Sheets of black opaque Tedlar are used to make the combined scintillator and white plastic sheets light-tight. Finally, a second 0.090" aluminum cover is located on top to provide a complete protective package.

The megatile unit is held and compressed together by a set of 0.188" diameter rivets spaced 18" or less apart. These rivets keep the inter-component gaps to ~0.015" or less so that fibers can't pop out of grooves and so that the reflective Tyvek paper is held right against the scintillator to minimize both the tile transverse response non-uniformity and tile to tile light cross-talk.

The SCSN38 scintillator megatile is constructed as follows: separation grooves between the tiles are cut into a 6 mm thick plate by a computer controlled machine, leaving ≈ 0.25 mm of uncut scintillator at the bottom of the grooves. The grooves are then filled with a white paint/epoxy mixture [17] to glue the individual tiles together. The epoxy is used for both the structural support and as a reflective surface at the edges of the tiles. A black marker is used to paint a line on the surface of the scintillator between the tiles to minimize the light cross-talk. Figure 9.15 shows the light cross-talk between neighboring tiles is less than 2% per edge of the tile.

After the glueing procedure is completed, the megatile is put back on the milling machine and the fiber grooves are cut out. In the next step, the scintillator sheet is wrapped using white reflective Tyvek. Then, a layer of plastic with grooves to route clear fibers is placed on top of the scintillator sheet. At the final assembly stage, the fibers are inserted into all tiles and the megatile is covered with black Tedlar for light-tightness and placed in aluminium pans for the mechanical protection. A full description of the assembly technique and quality control can be found
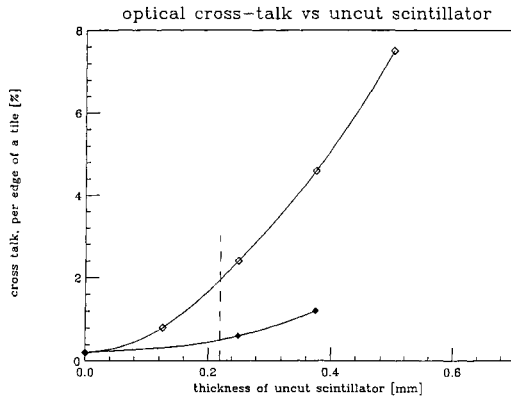
Figure 9.15: R&D studies on the optical cross-talk as a function of the thickness of uncut scintillator. The scintillator thickness was 6 mm. Open diamonds indicate the cross-talk when no black line mark is applied below the separation groove. Black symbols indicate the optical cross-talk for the tiles with a black line under the separation groove.

in [18].

9.5.4 Hadron Fiber Assembly Quality Control

Approximately 2600 fiber/connector assemblies (see section 9.6) are needed for the the hadron calorimeter. After mirroring, splicing and assembly into mass-terminated connectors, the fibers were tested by exciting them from the side with an UV lamp and measuring the light output at the unmirrored end using a photodiode. The lamp was moved in small steps along the length of the fibers and the response of the photodiode was recorded at each position. The peak wavelength of the UV lamp used in this setup was 405 nm: however a blue filter was used to remove the UV light of wavelength less than 385 nm.

By measuring the light yield of individual fibers, we checked the quality of the polishing, the reflectivity of the mirrored surface, the light transmission across the splice between WLS and clear fibers, and the quality of the connector surface. Figure 9.16 shows the distribution of the relative light yield of fibers as measured by the UV setup. The r.m.s. of this distribution is 3.2%. Fiber light yield was normalized to the average light yield of the set of fibers with the same length. Fibers with relative light yield more than 12% below the average were rejected. In those few cases, the particular WLS fiber was replaced and the entire connector was tested again. In some cases the low light
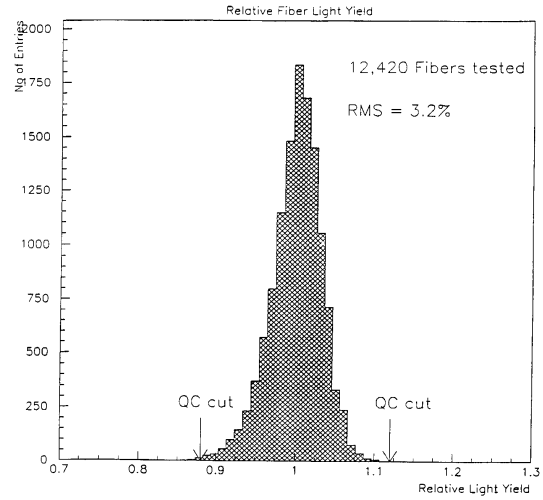

Figure 9.16: Distribution for the relative light yield of hadron calorimeter fibers assembled in the optical connectors.

yield of a fiber was related to a problem with clear fibers or connector parts. In these cases, the entire fiber/connector assembly was discarded and replaced by a new one.

In a sub-sample of 1600 fiber/connector assemblies, containing over 12,500 fibers in total, 85 fibers ($\approx$ 0.7%) were re-spliced and 40 fiber/connectors assemblies ($\approx$ 2.5%) were rejected. The average and r.m.s. mirror reflectivity, excluding fibers mirrored during a period of sputtering machine problems, were equal to 90% and 5.4% respectively. However, due to the attenuation of light in the WLS fibers, the typical increase of light yield for fibers with mirrored ends was between 30 and 40%. Thus, the contribution to the variation of the fiber light yield originating from the variation in the mirror reflectivity was $\approx$ 1.5-2%.

9.5.5 Hadron Tile/Fiber Assembly Quality Control

Prior to the shipment of scintillator material to Fermilab, the thickness of each scintillator plate was measured by the manufacturer, Kuraray International Corporation. The distribution of the average thickness of scintillator plates is shown in Fig. 9.17. The nominal thickness of the SCSN38 scintillator was 6 mm. Scintillator plates with average thickness below 5.8 mm were rejected by the manufacturer. The distribution of average scintillator plate thickness had an r.m.s. of 1.2%.

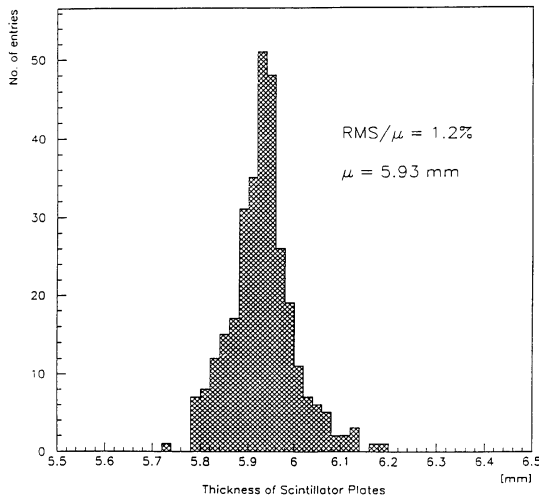To measure the variation in the absolute light yield

Figure 9.17: Distribution of average scintillator thickness used in the hadron pizza pan production.
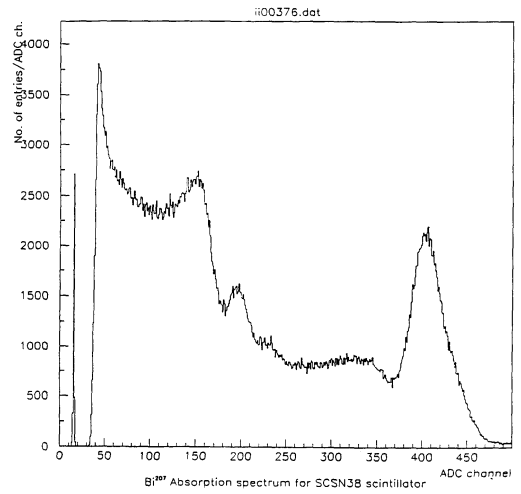
Figure 9.18: Absorption spectrum of the ^{207}Bi source used to check the light yield of the hadron scintillator plates before production. The position of the highest peak was used to determine the relative light yield of each sample.

of the scintillator material, we studied the scintillator absorption spectra using a ^{207}Bi source. Small 2 cm × 2 cm pieces of scintillator were placed on the face of the PMT and were excited with the β source. Figure 9.18 shows the ADC distribution of the PMT signal corresponding to the absorption spectrum of one scintillator sample. The light yield of each sample, relative to the reference sample, was measured by determining the position (in ADC counts) of the absorption peak corresponding to the largest deposit of energy. From this plot we infer that the distribution of the absolute light yield of scintillator plates had an r.m.s. of 1.6%.

After passing the UV light yield Quality Control (QC) test, the fiber/connector assemblies were inserted into the megatiles. Next, the megatiles underwent QC tests using a collimated ^{137}Cs γ source. We used a PC-controlled motor drive and data acquisition system to record the response of individual tiles to the radioactive source. The megatiles were placed inside a light-tight "scanner box" and positioned against three alignment pins. The relative light yields of the tiles were measured by recording the DC current response of a set of PMTs [1]. Data were taken in sequence by positioning the source over the geometrical center of each of the tiles in a megatile. The gains for the PMTs were measured before and after each megatile test using a control tile.

The r.m.s. of the relative gain of each tube measured during the period of QC tests described here (December 1993 through August 1994) was $\approx$ 0.7%-1.0%.

Figure 9.19 shows the distribution of the relative light yield for individual tiles from the first 14 layers. The r.m.s. of the distribution is 6.1%. The few tile/fibers assemblies with relative light yield less than 78% of the mean were repaired. In such cases, we either re-spliced the WLS fiber or replaced the entire fiber/connector assembly. During the production period, during which 378 megatiles were produced, with 1512 connectors and 12,420 fibers, 36 fibers ($\approx$ 0.3%) had to be re-spliced and 26 connectors ($\approx$ 1.7%) had to be replaced.

Therefore as a result of the two QC tests (UV fiber light yield and collimated γ source megatile light yield), 1% of the fibers were re-spliced and 4% of the fiber/connector assemblies were rejected and replaced.

A discussion of the possible sources of the tile/fiber assembly light yield variation is given in [19]. We can define the total variation of the relative light yield distribution, σ_{tot}, as:

$$\sigma_{tot}^2 = \sigma_{fib}^2 + \sigma_{meg}^2 + \sigma_{other}^2 \qquad (9.3)$$

where σ_{fib} is the relative fiber light yield variation (3.2%) and σ_{meg} is the variation of the average megatile light yield. We define the average megatile light yield as the average relative light yield of the
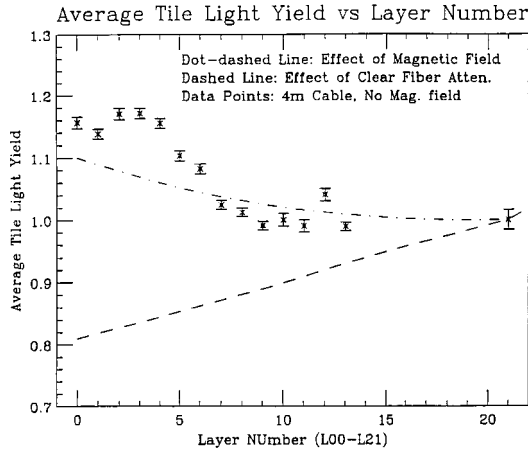
---

[1] Hamamatsu R580-17, 10-stage green-extended PMTs, operated at 1350 V, corresponding to a gain of approximately 10^6.

Figure 9.19: Hadron light yield for the first 14 hadron layers.

Figure 9.20: Transmission across fiber splices.

32 tiles belonging to a megatile. The term σ_{meg} describes an additional contribution to the tile light yield variation due to systematic factors common to all tiles cut from the same scintillator plate. The term σ_{other} corresponds to the light yield variation due to other factors. These factors include the quality of optical coupling of fibers inside the megatile and local variations in the scintillator material thickness. Using the measured values of $\sigma_{tot} = 6.1\%$, $\sigma_{fib} = 3.2\%$, and $\sigma_{meg} = 3.6\%$, we calculated $\sigma_{other} = 3.7\%$.

9.6 Optical System

9.6.1 Optical Fibers

9.6.1.1 Preparation of Optical Fibers

The optical system needed to route light from the scintillator tiles to the PMTs is a critical part of the Plug Upgrade Calorimeter. One of the most important components of this optical path is the splicing of each WLS fiber to a clear fiber of the same diameter for purpose of better light transmission. The splicing technique was developed to meet the following requirements:

- Transmission across the splice larger than 90%.

- Transmission variation less than 3%.

- Capability of splicing fibers of arbitrary length with no fiber damage.

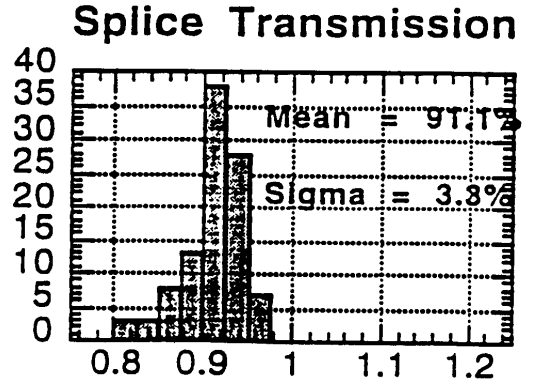- Operator-independent or nearly independent splicing machine.

Thermal fusion of plastic optical fibers had been shown to be an adequate technology during the construction of the engineering prototype [6] . For the full production of the hadronic fibers, a semi-automated splicing machine was developed. The central section of the machine includes a 250 W projector lamp to heat and fuse the fibers and two "half tubes" to constrain the fibers during heating. The use of half tubes makes it possible to splice any length of fiber without having to pull one fiber through a whole tube to remove it, a process that would be less efficient and more likely to damage the fiber. The half tubes are attached to bars, which are equipped with chucks to hold the fibers in position. To obtain consistent splices, fiber ends were polished to obtain a very uniform flat surface.

To determine the light transmission across a splice, a large number of Y-11 WLS fibers were cut and spliced approximately at their midpoints. The fibers were then excited transversely by a UV lamp and read out at one end by a photodiode. The difference in light yields for excitation on either side of the splice was used to determine the transmission. Figure 9.20 shows the results on a test sample of 100 fibers. The average transmission is 91%.

A sample of fibers were sent to University of Tsukuba for radiation testing. The splices exhibit no dependence on radiation doses up to 2 Mrad (see table 9.3).

Although the splice transmission is independent of fiber diameter, two characteristics do affect transmission through the splice [9]. The first is the type of cladding, which can be either single-clad or multi-clad. Any damage to the cladding during preparation of the fibers for splicing causes an increase in

the variation in light transmission. Single-clad fibers are more sensitive to cladding damage during polishing than multi-clad fibers.

The other characteristic affecting transmission is a property of the fiber core. The fiber supplier, Kuraray International, produces two versions of each fiber, distinguished as S-TYPE and NON S-TYPE, based on the orientation of the polystyrene chains. In the S-TYPE fibers, the chains are well oriented and the fibers are more flexible. The refractive index, however, is not completely uniform. In NON S-TYPE fibers the chains are fairly randomized and the refractive index is more uniform. The fibers are brittle, however, and easier to break if bent below a minimum radius. The NON S-TYPE fiber used for the hadronic calorimeter has a splice transmission approximately 10% higher than the S-TYPE fiber. A full description of the splicing machine can be found in [7].

Rad Dose (Mrad)	Trans.	Tensile Strength (Kg)	Bending Radius (cm)
Control	90%	3	11.5
0.3	92%	2.4	9.5
0.5	90%	3.2	11.5
1	87%	2	9
2	89%	2.5	8.5

Table 9.3: Results of radiation tests on fiber splices.

A similar splicing device has been developed for the EM calorimeter in Tsukuba. The fiber splicer heats the ends of the fibers inserted in a PEEK tube, which can help align the fiber axes and protects the fused joint mechanically. Since the tube itself is stiff, no structure to hold the fibers is necessary when the fibers are being pressed together during splicing. Various parameters such as the pressure, heating time, distance to the heater, were optimized and controlled by a PC. The transmission across the splice was found to be 95.8% with a r.m.s. spread of 1.3%, which was evaluated as the ratio between the light yield at the end of a piece of 1 m long clear fiber before and after a splice was performed on the middle point. A full description of the EM splicing machine can be found in [37].
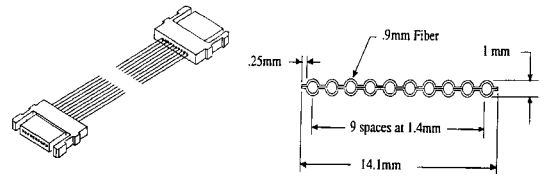

Figure 9.21: Schematic view of a 10-fiber optical cable assembly.

9.6.1.2 Optical Fiber Cables

As with ordinary electrical wires, a large number of optical fibers must be properly grouped to prevent confusion in connections and to provide mechanical protection. Protection of the fibers is important, since the fibers are routed over the end plug structure. We have developed optical fiber cables in which ten 0.9 mm diameter plastic fibers are assembled into a flat ribbon cable. The fiber spacing is 1.4 mm and there is a 50 μm thick protecting jacket made of black Tedlar [10]. The thickness of the jacket ensures enough flexibility in the fiber cable. Loss in light transmission has been tested as a function of the radius of curvature. The study also included an aging test performed using heat cycles. The results, similar to those observed with single fibers, showed no deterioration for radii of 1.5 cm or larger. Figure 9.21 shows a schematic view of a 10-fiber optical cable.

9.6.1.3 Optical Mass Connectors

To provide a convenient way of connecting and disconnecting the optical elements of the calorimeter, it was natural to terminate the optical fiber cables with connectors at both ends. The fibers from the tiles on a megatile are also terminated by connectors mounted on the outside edge of the pizza pan so that a pan is a single mechanical unit.

The most important feature of a connector is its reproducibility rather than its absolute light transmission. It was therefore decided to leave an air gap in the junction without optical grease.

There are two types of connectors: those used inside the EM pans are 3.2 mm thick $\times$ 28 mm wide $\times$ 26 mm long. They are closed by using specially machined shoulder screws which provide sufficient clamping force and precise location. The connectors are attached to the top external surface of the EM
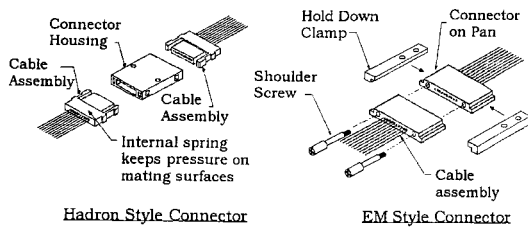
Figure 9.22: Schematic drawings of hadron (left) and EM (right) optical connectors.
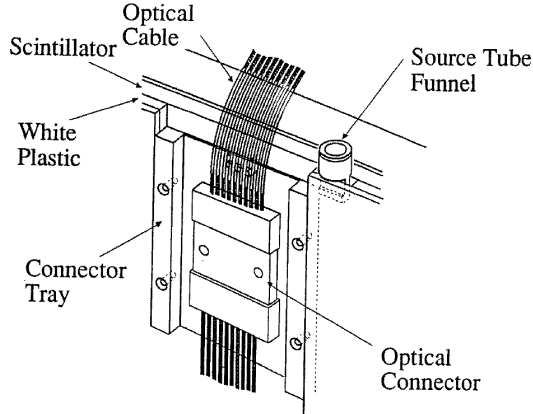

Figure 9.23: Mounting scheme of hadron optical connector on the outer edge of a pizza pan.

pans by clamping. A small L shaped "hold down clamp" screwed to the pan holds down the connector. The connector is set into the pan at a depth that allows the fiber bending radius to be sufficiently large while still remaining within the confines of the light-tight cover.

The 8.8 mm (.346 in.) longitudinal space allotted for the EM pans is not large enough to include both pans and connectors. The lead plates must therefore be cut away locally to create the necessary space for the connectors. Small pieces of tungsten replace the lead in these areas. These tungsten pieces, although thinner than the lead, are thick enough to provide approximately the same total interaction and radiation lengths as the lead they replace.

The shower maximum pans will use connectors identical to those used in the EM pans. These connectors are placed near the perimeter of the pans, some facing radially and some facing at 45° angles to the plug surface.

The hadron connector includes a spring clip assembly making connection and disconnection more convenient. The main features of the optical con-

nectors are shown in Fig. 9.22. Both connectors have been developed at DDK in Japan in conjunction with Tsukuba University and Fermilab, and have been tested both at DDK and Fermilab [38]. Additional space in the hadron section makes it possible to use a connector thicker than the one used for the EM and shower maximum pans. Connectors are fastened to hadron pans as shown in Fig. 9.23. An injection-molded "connector tray" is attached to the pan by sandwiching it between the scintillator and white plastic. The connector housing fits into the connector tray and is positioned by two holes. A cover (not shown) is screwed onto the tray, enclosing the connector housing. Cable assemblies then fit into the housing.

Extensive R&D studies have proven that the optical transmission of the connectors is adequate for our purposes. Approximately 10% of the light is lost due to the inevitable Fresnel reflection which is 5% at the boundaries between the fiber material (n=1.59) and the air gap. The average total light loss is 17%. The r.m.s. of the reproducibility is approximately 2-3%. It should be noted that the variation in light transmission of the individual light paths from the scintillator tiles in a tower is added in quadrature to the intrinsic tile response variation in the same tower. The variation of the light transmission of each light path in the cable connector assembly also affects the tower to tower uniformity.

9.6.1.4 Optical Fiber Routing

The flat fiber ribbon cables described previously route the light signals along the outside surface of the plug to connectors on the optical decoder boxes on the rear face of the plug. The fiber routing scheme is shown in Fig. 9.24. The pattern shown repeats every 15° of azimuth. Fibers from each portion of the detector maintain individual paths. EM fibers in the center are surrounded by hadron fibers, then shower maximum fibers, with the source tubes for all detectors on the edges of each 15° section. A 5 cm wide stay clear region every 15° allows for structural brackets. There is space for 10 rows of EM cables each 5 layers deep in the center.

Since there are only 46 EM cables, 4 empty slots in the EM section can be filled with cables from a proposed preshower detector. Hadron cables are stacked either 4 or 5 deep while shower maximum cables can be from 2 to 4 deep depending on their
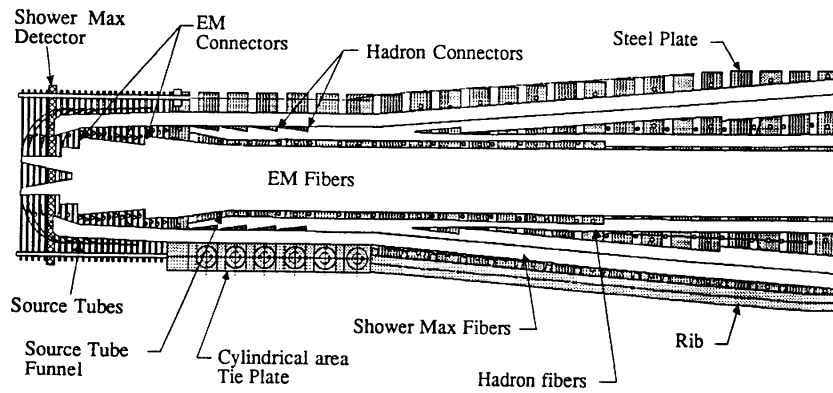
Figure 9.24: Fiber routing scheme on the outer perimeter of the plug. A 30° section is shown.

position. Stacks higher than 5 cables would result in fiber bending radii smaller than the 25 mm specified for the design. The cables must be held in place as they leave the pans and extend along the surface of the plug. Preformed pieces of foam rubber support the cables from above and below as they exit the pans. Brackets to hold down the fibers are attached to studs tack-welded to the surface of the plug. The studs are internally threaded so that light-tight covers can be attached to them.

The entire plug surface must be covered to physically protect the fibers and source tubes and to provide a light-tight enclosure. Covers will be made of .8 mm stainless steel sheet and will each cover 30° in azimuth.

9.6.1.5 PMT Placement

Approximately 1200 PMTs with their mechanical and electrical assemblies (base, light mixer, magnetic and electrostatic shields) and the associated optical decoder boxes for an end plug are grouped into 12 identical PMT boxes (Fig. 9.25) on the rear face of the plug.

The PMT boxes fit into a framework on the back of each Plug; each box can be mounted or dismounted separately of the others. Each PMT box allows space for the MAPMTs needed for the shower maximum detector. Internal to each box are additional subassemblies for the decoder boxes and the PMT mounting plates. The assembly was designed for manufacturability and ease of testing and replacement.

Each PMT box enclosure will be held at a temperature of 25°C and for this reason will be equipped with

a thermal control system [11]. At present, the plan is to use solid state thermoelectric devices for cooling and resistive heaters for warming if necessary. A plan for placement of the electronics and power supplies has been established and awaits final design decisions. The PMT box design has been finalized and the boxes are currently being produced.

Cables from the PMT assemblies will be routed inside the enclosure to mass connector blocks mounted on a patch panel. The panel has 10 signal connector blocks (10 channels each), and 12 high voltage connector blocks (8 channels each) associated with the R4125 PMTs. The signal and high voltage cable bundles will use RG-174 cable and crimp coaxial and pin connectors and block connectors similar to those used on the anode, dynode, and high voltage cables from the base packages.

9.6.1.6 PMT Mechanical Assembly

The PMT mechanical assembly and mounting arrangement were designed by Fermilab Technical Support Section physicists and engineers, in cooperation with the Michigan State University physicists and engineers who designed the decoder boxes onto which the PMT assemblies must mount.

Each PMT assembly will slide into an iron pipe screwed into the front plate of a decoder box. The PMT assembly is held in place by an aluminum cap, which presses against a plastic ring and a rubber O-ring. The O-ring makes the package light-tight at the cap end. At the light mixer end of the PMT assembly, the assembly engages with two holes in the "cookie" holding the light fibers bringing light from the calorimeter to the PMT. The assembly consists of

a mu-metal shield, a lucite light mixer, a base package, and several parts which allow the light mixer to be positioned precisely with respect to the cookie surface, leaving a small air gap (2 mm).

As soon as a PMT/base combination has passed all tests, the PMT and base network are built into a complete assembly.

9.6.2 Photomultipliers

9.6.2.1 Single-Channel PMT

The original specifications of the single-cathode PMT to be used for the EM and hadron calorimeter portions are listed here.

- The diameter of the PMT must be less than 40 mm.

- The photocathode should be a green extended bi-alkali with a quantum efficiency of at least 12% at a wavelength of 520 nm.

- The gain times quantum efficiency should be 3.75×10^5 for EM tubes for an operating voltage less than 95% of the maximum rated value.

- The gain times quantum efficiency should be 3.75×10^6 for hadron tubes for an operating voltage less than 95% of the maximum rated value.

- The gain times quantum efficiency should meet previous specifications for an operating voltage less than 2000 V, and all PMTs must have operating voltages within 20% of the mean operating voltage for their respective types.

- The gain times quantum efficiency should be constant to within 2% for anode charges of 750 pC/pulse (corresponding to a peak current of 30 mA for a triangular pulse with a 50 ns base).

- The gain times quantum efficiency should be stable within 1% over any 24-hour period for a constant anode current between 100 and 500 nA at constant temperature after an initial burn-in period of 40 hours.

- The gain times quantum efficiency should have a temperature dependence of less than 0.4%/ °C.

- The gain times quantum efficiency should not change by more than ± 1% after the voltage has been ramped from its nominal operating value to 300 V and back to the operating voltage.
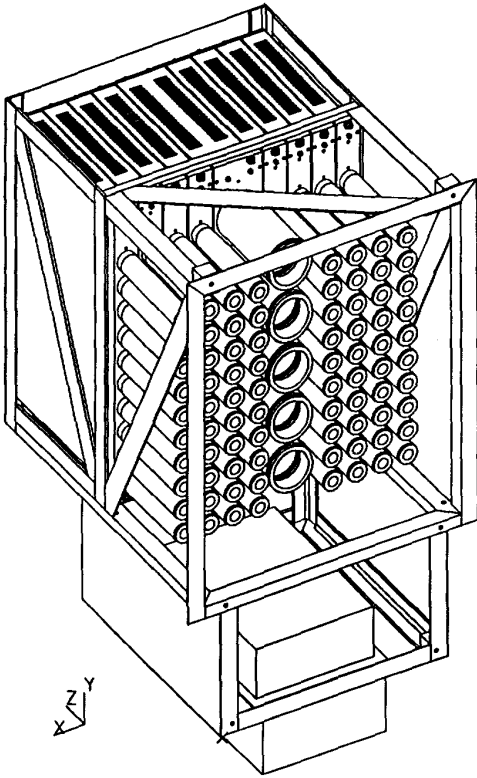

Figure 9.25: Drawing of a fully loaded PMT box. 12 PMT boxes house all the PMTs for an endplug and are mounted on the back face of the plug.

- The gain times quantum efficiency should not change by more than ± 1% for pulses as little as 130 ns apart.

- For an instantaneous light flash the duration of the output pulse (FWHM) should be less than 20 ns for a load of 50 Ω.

- The dark current should be less than 1.5 nA when the PMT is at operating voltage.

- The minimum lifetime of the tubes should be greater than 3 years at an average anode current of 25 μA.

Small groups (about 10 each) of several commercially available candidate PMT types were evaluated by Technical Support personnel at Fermilab during 1992 and 1993 [22]. Tests of gain versus voltage, dark current, relative quantum efficiency, pulse height resolution, stability, linearity, temperature dependence, and photocathode uniformity were performed at Lab 2. The PMT ultimately chosen for the EM and hadron portions of the calorimeter was the Hamamatsu R4125, a 18.6 mm diameter 10-stage PMT with a green-extended bi-alkali photocathode and K-Cs-Sb dynodes [23].

In the section on PMT testing below, a subset of the PMT performance specifications will be discussed. The complete performance specifications for the Hamamatsu R4125, which were the result of discussions between Plug Upgrade personnel and Hamamatsu Corporation representatives, can be found elsewhere [24]. Delivery of the initial order of 2100 PMTs began during December 1993 and was completed in April 1995.

9.6.2.2 Single Channel Phototubes (PMT) Bases

The base for the R4125 was designed at Fermilab and built by Thorne EMI Corporation; the socket connectors, however, were purchased from Hamamatsu Corporation (part number E678-12H). Design considerations and the details of the circuit have been documented previously [25]. The base network circuit is a conventional resistive chain with ballast capacitors. The circuit has both final dynode and anode outputs. Only the anode outputs will be used in Run II.

The base does not include a "protection network" to limit the build-up of charge on the anode if the PMT is turned on while the anode is not terminated.
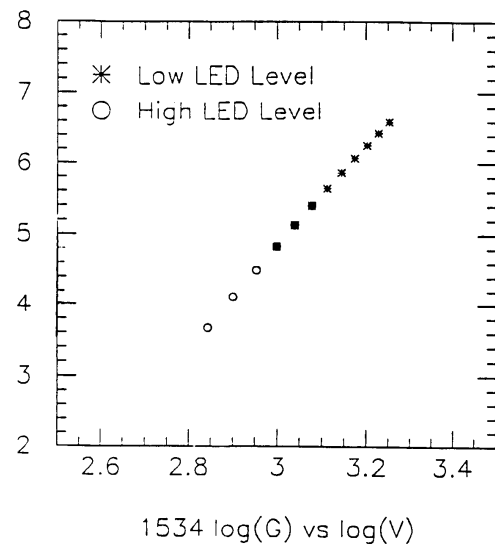

Figure 9.26: Typical R4125 single-anode PMT gain measurement as a function of the operating voltage (1534 is the tube ID).

Instead, this will be done at the anode cable termination at the front end electronics crates.

To keep the base package physically small, surface mount resistors and capacitors were used in the fabrication. To further reduce bulk, RG-174 coaxial cable was chosen for the anode, dynode, and high voltage cables coming out of the base package. Connectors were added to the anode, dynode, and high voltage cable ends by Technical Support personnel. Crimp coaxial connectors (AMP part 226537-1) were attached to the anode and dynode cables. Crimp pin connectors (AMP part 66103-4 for signal, and 66099-4 for ground) were attached to the ground and signal conductors of the high voltage cables. Delivery of 2100 bases was completed in early 1995. All bases were tested by Technical Support personnel during 1995. Only one base had to be returned to the manufacturer for replacement.

9.6.2.3 Single Channel PMT Testing

The 2100 PMTs purchased for the EM and hadron calorimeter are being tested at Fermilab and in Bologna, Italy. Testing is performed in two phases, called "pretest" and "full test". For the "pretest", each PMT/base combination has its gain versus voltage behavior measured. The PMT is then "conditioned" for 48 hours by exposure to steady-state LED light sufficient to produce 2 μA of anode current at
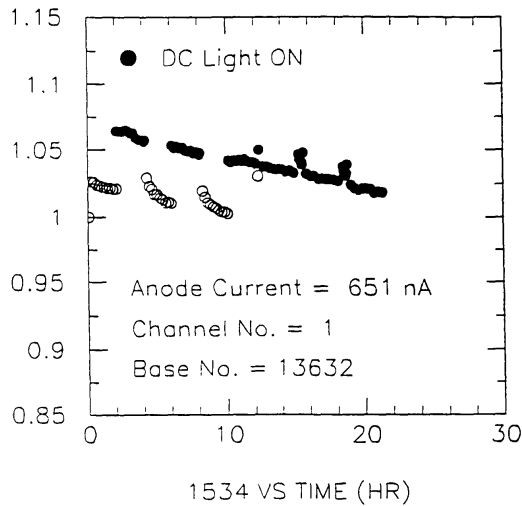
Figure 9.27: A typical R4125 PMT response to the "pulse-DC" and "high voltage ramp" tests. The response of the PMT to pulsed light as the DC background light is cycled is seen in the first 12 hours. At approximately 14 and 18 hours the response change due to cycling the PMT supply voltage is shown.

Figure 9.28: Typical R4125 single-anode PMT stability test over a period of 115 hours.

a gain of approximately 5×10^4 (the nominal EM calorimeter gain.) The entire initial order of PMTs was pretested at Fermilab during 1993 and 1994. For the "full test," a number of tests are performed on each PMT/base combination:

Gain versus Voltage: The gain is measured using the "statistical method" [26] at a value of the high voltage that gives a gain close to 10^6. This value of the high voltage is referred to as the "anchor point." Gains at a range of voltage values between 1800 V and 700 V are measured by comparing the average output for 10,000 flashes of the LED system at each voltage with the average output at the anchor point. The dark current of each PMT/base combination is measured at voltages between 700 V and 1800 V. Figure 9.26 shows the gain versus voltage behavior of a typical PMT.

Stability: Three kinds of stability test are performed, all at a gain of 5×10^4. The "pulse-DC" test is a measure of how much the response of a PMT shifts with changes in average anode current. The "high voltage ramp" test measures how long it takes for a PMT to return to within 2% of its nominal response after its high voltage has been reduced to 100 V for 1/2 hour. Figure 9.27 shows the behavior of a PMT in the "pulse-DC" and "high voltage ramp" tests. The PMT response shifts by 4.3% when the DC
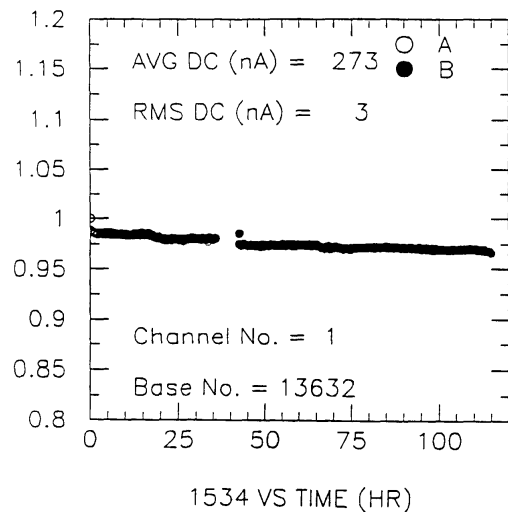
light is turned on (the specification calls for a shift of no more than 5%). The deviation from nominal response after high voltage restoration is also visible in the figure, but the PMT returns to within 2% of its nominal response within 2 minutes of high voltage restoration (the specification calls for no more than 10 minutes waiting time).

The "long stability" test measures the variations in PMT response to pulsed light over a 72-hour period. Figure 9.28 shows the behavior of a PMT during the long stability test. The vertical axis shows the response of the PMT normalized to its initial value (the gap in the data indicates a period during which data were not recorded due to a computer error). The response of the PMT varies by at most 1.6% over any 48-hour period in the test.

Linearity: early tests on the R4125 showed them to have excellent linearity behavior [27]. After the "long stability" test, the gain versus voltage behavior is remeasured, and linearity is measured at four values of the gain, namely $1 \times 10^4, 5 \times 10^4, 1 \times 10^5$ and 5×10^4, The figure of merit for the linearity measurement is the peak anode current at which a PMT departs from linear output (output proportional to the input light level, as independently measured by a PIN diode) by 2%. Figure 9.29 shows the behavior of a PMT at gain 5×10^5. The PMT output falls 2% below its linear output at a peak anode current of 88 mA, a value which lies above the specification of 70 mA at this gain (the apparent non-linearity at very low peak
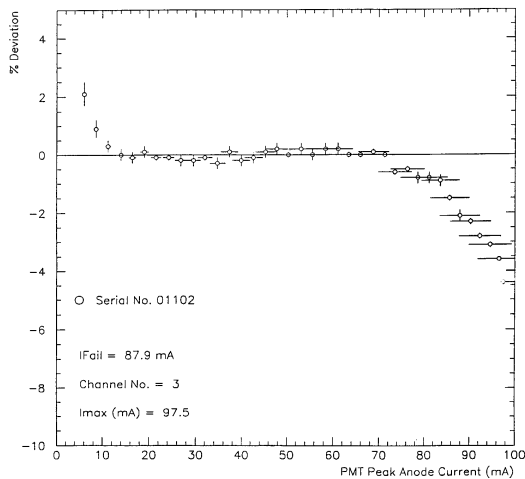
Figure 9.29: Percentage deviation from linearity for a typical R4125 single-anode PMT.

anode current is due to the PIN diode, and not the PMT).

Relative Quantum Efficiency: At Fermilab, a subset (about 8%) of the PMTs have their relative quantum efficiency measured. This test is done with a tile/fiber system. The measure of relative quantum efficiency is the number of photoelectrons (N_{pe}) produced by the standard tile/fiber combination. N_{pe} is measured for the three PMTs having lowest cathode blue sensitivity (a parameter measured by the manufacturer) from each "batch" of PMTs tested. In this manner, we measure the "worst case" relative quantum efficiency subsample from each batch. So far, no PMTs have been found with unacceptably poor relative quantum efficiency.

9.6.2.4   Multi-Anode PMTs (MAPMT)

The SMD and the preshower detector are read out using WLS fibers which are 0.83 mm in diameter at the detector level and 1 mm in diameter when they reach the read-out region. In total there are 6400 strips and approximately 1000 preshower tiles to be read out, with limited space available for the photon read-out. The Multi-Anode PMTs responsible for the photon readout of the 6400 SMD scintillator strips must meet the requirements summarized in Table 9.4.

The possibility of using MAPMTs for the photon readout of SMD is one we have been investigating for several years[5]. The first generation of MAPMTs, such as the Hamamatsu 4135A, were plagued by high channel to channel cross-talk and limited dynamic

Gain	10^6
Quantum Efficiency	10%
Pixel to Pixel Cross Talk	$\leq 5\%$
Dynamic Range	500
Photocathode Uniformity	33%
Rate Capability	10^6Hz
% Dead Channels	0
DC output	yes

Table 9.4: MAPMT Requirements

range [28]. The second generation of tubes, such as the Hamamatsu 4140 and Philips XP1702 [29], are significantly improved in these areas, but still have low quantum efficiencies and large channel to channel gain variations.

A third generation of MAPMTs from Hamamatsu has recently become available for testing. We evaluated two of the newest types of MAPMTs: the R6246, an 80 channel tube, and the R5900-M16, a 16 channel tube. Both types use a metal channel plate dynode structure, and have greatly improved performance compared to the previous generations of MAPMTs. The cost per channel and the superior channel to channel gain uniformity drove the selection of the R5900-M16 tube for the photon readout of the SMD.

9.6.2.5   Description of the MAPMT and Test Results

The 16 channels of the R5900-M16 are arranged in a 4×4 grid, which is contained within a 28×28 mm^2 square package 31.5 mm deep, including the vacuum nipple. The tube is of the head-on type, with a metal envelope held at the cathode potential. The dynode structure is the metal channel plate type developed by Hamamatsu, and the window is made of borosilicate glass, with a bi-alkali photocathode. The tube can be operated with negative high voltage for DC-coupled anode output, with gain as high as 1.5×10^7 at the maximum operating voltage of 1000 V. The 16 pixels are arranged in a square grid, with uniform pixel to pixel spacing of 4.5 mm. The manufacturer's specification sheets show that the spectral response is strongest between 300 and 650 nm, and that the peak cathode luminous sensitivity is typically 70μA/lm.

The 16 pixels share a common 12-stage dynode structure. We tested tubes with both linear and tapered (1.5:1.5:1.5:1:1:...:2:3.6) base resistor chains.

The total resistance of the linear and tapered bases were 2.6 MΩ and 4.0 MΩ, respectively, implying maximum base currents of 380 and 250 μA at 1000V. The signal output pins are connected to ground through the 50Ω termination provided by the ADCs used in the readout.

The single photoelectron distributions were measured at Fermilab. The first series of tests mapped the response of individual pixels and relative gains of the tapered base tube at operating voltages of 650 and 750 V. According to the manufacturers test sheets, these voltages correspond to overall gains of approximately 10^5 and 5×10^5. During the mapping of individual pixels, all 16 pixels were read out, and the tube face was scanned in 0.25 mm steps. An LED was flashed 60 times at each fiber position with intensity corresponding to approximately 2×10^3 pe output from the photocathode, while the ADCs digitized the anode outputs from each flash. At the end of each step in fiber position, the mean and r.m.s. responses of all 16 channels were recorded.

The spatial response of a typical single pixel is shown in Fig. 9.30. The typical areas for response greater than 90% of maximum are 1.5×2.0 mm^2. The relative responses of all the pixels are plotted in Fig. 9.31, using the point of maximum response, rather than the response measured at a fixed pixel pitch. The inset shows the relative responses measured for each pixel's local maximum relative to the pixel with the highest response. The uniformity was quite good compared to earlier generations of MAPMTs, and did not significantly change between the two operating voltages. The minimum pixel response was 56% of the maximum pixel response.

The relative gains were also measured for this MAPMT using the response at the geometric centers of the pixels. That distribution was less uniform, with the response of the lowest gain pixel 42% of that of the maximum response pixel; still within the 3:1 limit of our specification, however.

The linearity of the R5900-M16 was measured at a gain of 10^5 for output charges between 5 pC and 200 pC. The output for the tube with the linear divider dropped by about 10% for outputs of 100 pC, at a gain of 10^5, which is marginal performance for our application. With a tapered voltage divider in the base, however, the R5900-M16 showed typical devi-
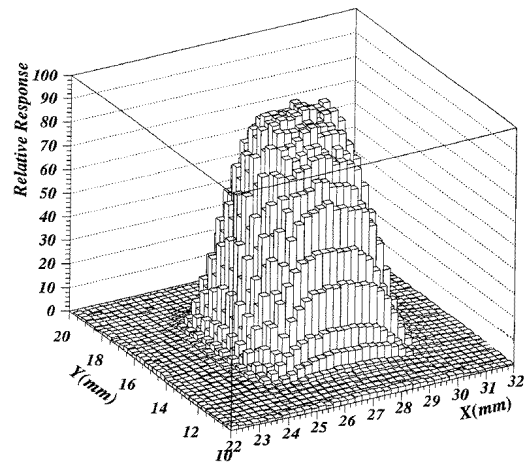

Figure 9.30: MAPMT single pixel response to an illuminating fiber scanned over the pixel surface in steps of 250 μm.

ations of less than 5% for output charges as high as 200 pC.

Pixel to pixel cross-talk values were measured by positioning the fiber over the maximal response point of each pixel and reading out all 16 channels. Signals in adjacent channels were gain-corrected and normalized to the illuminated pixel. The cross-talk values are shown in Fig. 9.32. The nearest-neighbor pixels' mean cross-talk was 0.7% and the median was 0.4%. In the diagonal neighbor pixels the cross-talk values averaged less than 0.2%, with a median of 0.09%.

Data taken at the geometric center of the pixels showed no nearest neighbor cross-talk greater than 2%, and the high cross-talk entries in Fig. 9.32 are the result of the variation in the position of the maximal pixel response.

The MAPMTs will be used in an environment that has changing background light levels, and which may require cycling of the operating voltage. For these reasons, the gain stability of the MAPMTs was tested under several conditions. The operating voltage may need to be turned off to prevent damage from large signals at the beginning of a Run II store. The response of a MAPMT should be stable within 10 to 20 minutes after having been turned back on so that no data are lost at the beginning of data taking. The MAPMT response returned to within 1% of the response before the voltage was turned off within 10 minutes of the voltage being turned back on, which is adequate for our purposes.

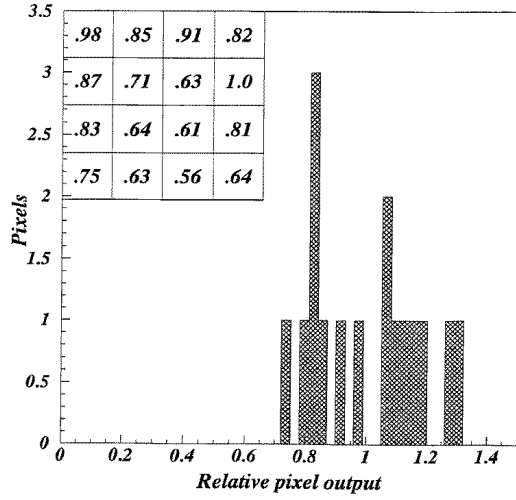In our application the MAPMT pixels will see

Figure 9.31: Relative responses of the 16 pixels of a MAPMT (Hamamatsu R5900-M16).
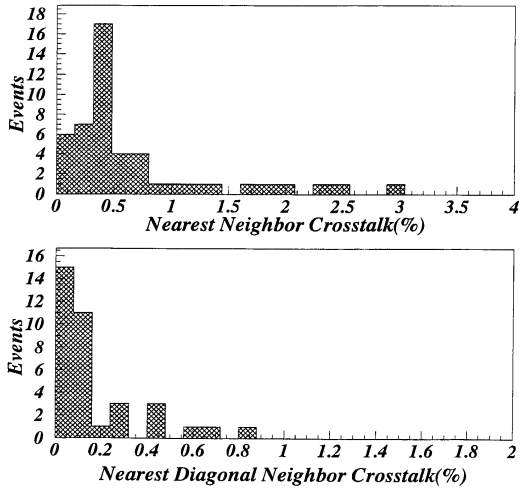

Figure 9.32: Percentage of optical cross-talk between a pixel and its neighbors (Hamamatsu R5900-M16).

quasi-DC light levels sufficient to produce currents from 1 to 100 nA per pixel. Within this range, the average current of a pixel will depend on the position of the corresponding scintillator strip in the SMD; the current will also change during the course of the store and the course of RunII. It is therefore important that the response to large pulses not depend strongly on the background current.

Two tests were performed, each over a period of about 48 hours, using average LED-induced background currents of 10 nA and 1 μA per pixel. The background LED was switched on and off at two hour intervals. For the higher background current, the shift in response to pulses when the LED was switched on and off was still less than 3%. At the lower level, the effect of switching the LED on and off was not observable, although there was a gradual downward drift of about 2% over the 48-hour period of the test.

Our final test compared the R5900-M16 response to a very low light level with that of a reference PMT (Phillips 2081B) having quantum efficiency of about 20% at a wavelength of 500 nm. A plot of the response is shown in Fig. 9.33. Single and double pe peaks are clearly visible, indicating small gain dispersion in the electron multiplication process. The operating voltage was 1000V, corresponding to a gain of approximately 10^7. The ratio of the quantum efficiencies of the MAPMT and reference PMT was derived from the fractions of events in the pedestal bins, which should be exp($-\mu$), where μ is the mean number of pe produced. In the case of Fig. 9.33, the R5900-M16 plot corresponds to a mean response of 1.06 pe, while the 2081B reference tube gave 2.03 pe for the same illumination. Since the quantum efficiency of the 2081B for 500 nm light is approximately 20%, we infer that the R5900-M16 quantum efficiency is approximately 10%. Both the gain dispersion and the quantum efficiency of the R5900-M16 are considerably improved over those of fine mesh type and other previous generation MAPMTs.

For the preshower detector, at gains of 1×10^5 and luminosity of $\simeq 1 \times 10^{32}$ cm^{-2}s^{-1}, the anode current for the highest η region tiles can reach approximately 0.7 μA due to the overlap of particles from different minimum bias events [40]. The signals of the 16 preshower counters at the smaller η region in a 15° pan are fed to a single MAPMT. The rest of 4 signals in the higher η region are read out by another MAPMT, together with those from three other 15°
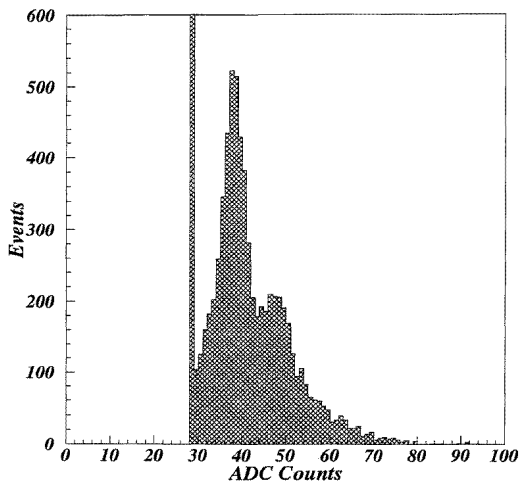
Figure 9.33: Single and double photoelectron peak response for the Hamamatsu R5900-M16.

pans. The anode current of the MAPMT used for the higher η tiles will be $\simeq 8\mu A$ at the conditions described above. Tests performed at the University of Tsukuba showed that a linear base for the preshower MAPMT will perform adequately.

9.6.2.6 High Voltage System

The high voltage power supply that will be utilized in the Plug Upgrade is a system recently made available on the market by CAEN [41]. It is a highly modular system, called SY527,consisting of a Crate (Mainframe) that lodges HV generator "plug in" cards of many different kinds. A single Mainframe can lodge up to a maximum of 10 cards of the same kind. The configuration that optimizes costs and performaces still fulfilling the needs, for both the Plug Calorimeter and the Preshower and Shower Max. detectors, was found to be the one based on the an active distributor card called A932 N. The A932 N card fans out the input high voltage to as many as 24 output channels, allowing at the same time a certain amout of high voltage regulation on each output channel; in fact each channel can be independently regulated and monitored within a range of 1000 volts, starting from the input voltage down. Moreover this kind of card encompasses one HV active generator besides the 24 distributed channels thus avoiding the need for an external power supply. The resolution is 0.2 volts . The maximum current is 0.5 μa at 2.5 kV. The active channel can reach 2.5 kV with a maximum of 13 mA.

To optimize the system for the HV need of the plug PMTs and MAPMTs, we need 2880 HV channels, corresponding to 12 Mainframes and 120 cards. At the present time 5 Mainframes and 65 cards are procured. The total hardware procurement will be completed by the midde of 1997.

Long term stability as well as linearity and (absence of) ripples are checked on each individual mainframe and card at the University of Bologna.

9.7 Stability Monitor

The calorimeter response will need to be stable over long periods of time to avoid repeated calibrations. Since the calorimeter response can be compromised by any one of many elements in a long chain, it is necessary to monitor the stability of response continuously, starting at different points in the chain to distinguish between different effects. One needs to distinguish between degradation of the scintillator or the optical transmission elements, such as may be produced by ageing or by radiation damage, and changes in the electronic amplification and digitization system.

Since the EM and hadron calorimeters have been designed to have resolution of $16\%/\sqrt{E}$ and $80\%/\sqrt{E}$ respectively with a constant term below 1% in the EM detector, the stability must be monitored to better than 0.5%. The stability in the amplification/digitization system will be monitored using a system based on the fiber-optic distribution of laser-generated light to all single-anode and multi-anode PMTs.

9.7.1 Design Criteria

The system must be capable of monitoring the stability of $\simeq$ 2100 phototubes to better than 0.5% over a period of years. It should mimic the calorimeter signal as closely as possible, with a rise time of several ns and a fall time of 20 to 50 ns, and it must have a high degree of redundancy.

The system is based on the distribution of light pulses from a single light source to all the PMTs. The use of a single source is advantageous in that it leads to channel-to-channel correlations (both in time and amplitude) which can be exploited during setup and diagnosis. The power requirements can be quantified in terms of the number of photoelectrons produced at the photocathode by a typical signal (e. g. a signal corresponding to 50 GeV deposited in a calorimeter
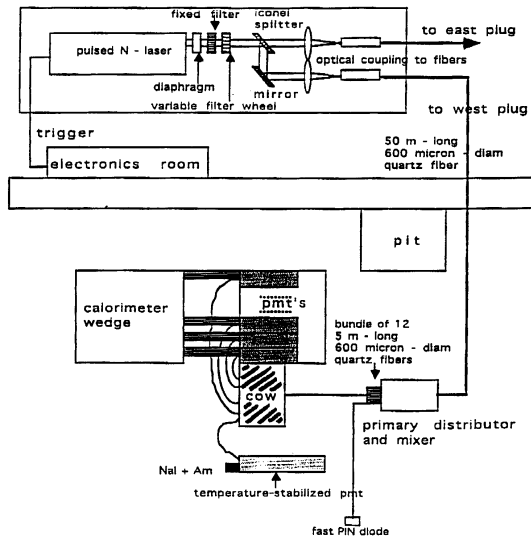
Figure 9.34: Schematic drawing of the laser stability monitoring system.

tower). Given the response expected from the EM and hadron calorimeters (approximately 350 pe/GeV and 19 pe/GeV, respectively), 50 GeV corresponds to about 2×10^4 pe in the EM calorimeter and about 1×10^3 pe in the hadron calorimeter. It is useful to note that, if the resolution σ is determined by Poisson statistics, i.e. if $\sigma = \sqrt{1/n_{pe}}$, then the power requirements corresponding to a convenient (50 GeV) pulse amplitude also correspond to statistics which are sufficient to monitor stability on a pulse by pulse basis.

Pulsed lasers emitting in the UV range satisfy these requirements as well as the need to mimic the calorimeter pulse shape; the wavelength (337.1 nm for the laser chosen) is short enough to excite a piece of scintillator similar to the one used in the calorimeter, and the pulses are narrow enough (generally < 5 ns) that the pulse shape will be determined by the WLS used for light distribution as described below. On the other hand, the 3% pulse to pulse fluctuations typical of such lasers need to be factored out: this is an essential aspect of the system.

9.7.2 Description of the Laser Light Distribution System

Light generation, transmission, and distribution for the stability monitor system are illustrated schematically in Fig. 9.34 and may be summarized as follows:

- the laser beam is split into two beams at the source

- the two beams are coupled into 600 μm-diameter quartz fibers; one for each plug

- each beam is transported 50 m to the primary distribution point

- at the primary distribution point a beam is "mixed" and distributed to each of 12 secondary distribution points ("cows")

- in each cow, the UV light excites a scintillator and the light emitted by the scintillator is distributed to each of 100 WLS fibers;

- the WLS fibers emission peak is at 520 nm and a part of this emission is captured by the fiber and transmitted to a single PMT. In this way, all PMTs are excited by each flash of the laser.

The plastic scintillator inside each cow (Fig. 9.35) emits light at an average wavelength of 420 nm, with a quantum efficiency of 90%. Approximately 25% of the scintillation light is emitted into a cylindrical reflective cavity and reaches the edge, along which are distributed 120 0.83 mm diameter WLS fibers, at intervals of 5 mm. The WLS fibers are of the same kind as those embedded in the tiles of the Plug Upgrade Calorimeter. Of the light reaching the edges of the cavity, 17% (0.83 mm/5 mm) is incident on the 120 WLS fibers and each fiber receives approximately 1% of this light which it converts to 520 nm light within the WLS fiber with an efficiency of 70%. The light is emitted isotropically so that only $\sim 8\%$ is captured in the fiber and 50% of this light travels towards the PMT.

This light is transmitted to a 0.9 mm diameter clear plastic fiber by means of the optical connector (section 9.10) and transported 1.5 m to a second optical connector at the interface of one of the decoder boxes. There the 0.9 mm-diameter clear fiber connects to a 1 mm diameter clear fiber. Inside the decoder box each 1 mm diameter clear fiber is incorporated into a bundle of fibers corresponding to a calorimeter tower and optically connected to a PMT. The attenuation introduced by the clear plastic fiber and the two optical connections is estimated to be 50%.

The intensity of the 520 nm light which eventually reaches the PMT cathode is therefore estimated to be $0.9 \times 0.25 \times 0.17 \times 0.01 \times 0.7 \times 0.08 \times 0.5 \times 0.5$ that of the UV light reaching the cow, which corresponds to an attenuation factor A_{cow} of $\sim 5 \times 10^{-6}$. Using this
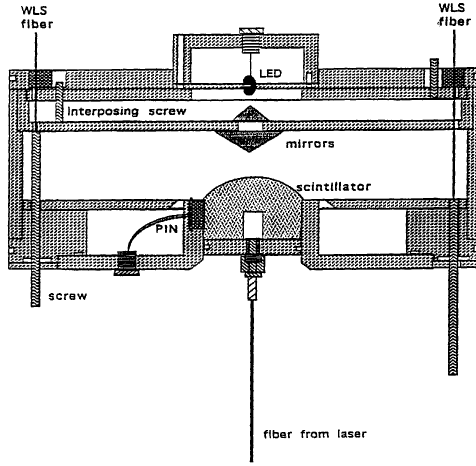
Figure 9.35: Cross-section view of a stability monitoring system secondary light distribution module (COW).

estimate for the attenuation introduced by the cow, and adding in the measured attenuation of the system from the laser to the cow, the overall attenuation A in the distribution system will be: $A = 1.3 \times 10^{-8}$. Given an intensity $L = 4.7 \times 10^{14}$ photons per pulse at source (corresponding to a Photonics LN300 nitrogen laser), the number of photons per pulse reaching the photocathode should be $n_{ph} = 6.2 \times 10^{6}$ and assuming a photocathode quantum efficiency of 20%, one should obtain a *maximum* of $n_{pe} = 1.2 \times 10^{6}$ photoelectrons per pulse. Assuming the calorimeter response values quoted in section 9.7.1, this corresponds to a single tower energy of about 3 TeV in the EM section.

The laser intensity fluctuates with a standard deviation σ_L of about 3% from pulse to pulse. This fluctuation is transmitted to the scintillator emission in each cow and, assuming that the scintillator emits isotropically, to each detector viewing this emission. In order to factor out these pulse to pulse laser fluctuations, one must include, amongst the detectors viewing the scintillator emission, at least one stable reference detector. The ratio R between the integrated charge Q_{PM} in the PMT corresponding to a calorimeter channel i and the reference detector charge integral Q_D should then be insensitive to the laser fluctuations. However, statistical requirements must be modified to take the reference detector into account; the fractional variation in pulse to pulse fluctuations of this ratio,

$$\frac{\sigma_R}{R} = \sqrt{\left(\frac{\sigma_{Q_{PM}}}{Q_P}\right)^2 + \left(\frac{\sigma_{Q_D}}{Q_D}\right)^2} \qquad (9.4)$$

must be smaller than 1%.

We have already established that power requirements corresponding to a 50 GeV calorimeter signal are compatible with pulse by pulse stability monitoring. If we want to preserve this capability, we must ensure equal or better statistics in our reference monitor, i.e. $\sigma_R/R <\sim 1\%$. Two such reference monitors have been designed into the system for redundancy. The first is the set of two PIN photodiodes indicated in Fig. 9.35. Though the PIN photodiodes [31] are expected to be very stable with respect to temperature change (0.003% /$^{\circ}$C), a temperature monitor was included in each cow. This will also allow eventual effects of temperature-dependent mechanical stress on the light distribution to be monitored. The second reference monitor is a temperature-stabilized PMT which simultaneously views one of the fibers from the cow and an ^{241}Am-loaded NaI scintillator. The stability of the PMT response is monitored with reference to the 5.4 MeV ^{241}Am α -peak in the signal from the NaI scintillator. Residual temperature-related instabilities arise from the temperature dependence of the NaI response ($\sim 0.2\%/^{\circ}$C) [32]. The temperature of the PMT must be stabilized to better than 2°C.

9.8 Calibration Scheme

9.8.1 Calorimeter Calibration

Measurements performed on individual tile responses and PMT gains described previously will allow us to know the absolute response of a given tower to approximately 30-40%. In the hadron calorimeter we plan to reach a calibration level of the order of 3-5% with a combination of muon calibration and wire-mounted source calibration. For the EM calorimeter we will use the same methods for a preliminary calibration, but during the course of data taking we will be able to shift to a calibration based on physics signals such as $Z \to ee$. We could also use $J/\psi \to ee$ decays provided CDF can track at large η and we can trigger on them.

We have investigated in the past a calibration scheme for low energy electrons based on the reconstruction of $\pi^0 \to \gamma\gamma$. By measuring the photon energies in different towers and using the shower max-

imum detector to measure the opening angle we obtained some promising results. An extensive study of calibration methods based on the exploitation of physics signals awaits the integration of the Plug Upgrade Calorimeter into a full CDF detector simulation. Here we discuss the calibration scheme based on muons and the wire-mounted source.

9.8.2 Moving Radioactive Sources

The wire-mounted source system is an important part of the calibration system for the CDF Plug Upgrade Calorimeter. The ^{137}Cs source of about 4 mCi is mounted inside the tip of a long flexible stainless steel wire. The source is "parked" inside a lead brass shield on the wire source driver when not in use. The wire is curled several turns on a reel with radius 5 in. The driver uses two motors to direct the wire source into the calorimeter. One motor controls the source tube selection and the other actually drives the wire source along the tube.

The wire source system will be used in the cosmic ray and test beam tests . Data from these tests along with those obtained during megatile production will be used to determine the initial gains of the towers of the fully installed detector at B0. All the layers in the final calorimeter can be source tested when the plugs are pulled out. The following layers can be source tested at any time: the preshower and shower maximum layers; four layers (2, 4, 6, 16) of the EM calorimeter; four layers (0, 6, 12, 19) of hadron calorimeter.

To sample and calibrate these layers when the detector is installed at B0, four drivers will be mounted on the back of each plug, each serving one quadrant. To provide a secured path for the source from the driver to the megatiles, two kinds of tubes will be used. One is stainless steel tube, routed on the outer perimeter of the plug along with the optical fiber cables. One end of each tube is coupled to the tube embedded in the megatile; the other end extends out of the edge of the plug. A flexible nylon tube provides a bridge between the end of the steel tube and the indexing disk of the source driver.

It will take about 30 minutes to scan the frontmost layer (preshower); less time will be required for the back layers. During plug assembly a PC-based stand-alone data acquisition system will be used to test the tiles with the wire source. This system controls the source driver and reads out the position of the wire-mounted source as well as the tile response to the source through ADCs. The ADCs can be read by the PC either through CAMAC or through expansion cards inside the PC. After the detector is commissioned, the PC will still be used to control the source driver mechanism, but the ADC readings will be done by the CDF main DAQ system. The PC will also provide the wire source position to the main DAQ.

In principle, the source calibration could substitute for test beam exposure since:

- every tile has a measured ratio of collimated source to wire source

- the collimated source response should correlate well with either MIP response or hadron response

- every tile can be wire sourced after the final optical cabling and phototubes are installed.

The source calibration can be used to transfer the calibration from the Test Beam tests to B0. However, with the magnetic field on (plugs closed), only a few layers can be scanned with the wire-mounted source. These few layers can be used to determine the effect of the magnetic field on the scintillator.

The primary calibration will be in terms of a minimum ionizing muon signal. That is, all towers will be calibrated relative to one another using the most probable energy deposition, summed over all 22 layers, of a minimum ionizing muon (defined to be a MIP) and shower energies will be expressed in terms of MIPs.

This μ calibration will be obtained for all the EM towers in the full calorimeter using cosmic rays, and for a 60^0 mockup section (see section 9.9) of the hadron calorimeter in the beam test. Since the muons in the test beam will have higher energy than those at B0, the energy dependence of the muon response will be checked by measuring the response of the EM test beam section to both cosmic rays and test beam muons. Data from CCFR [33] and Hanging File experiments [34] indicate the most probable energy deposition of muons in a calorimeter increases by 7% for every 100 GeV of muon energy.

In our design, a muon signal has the same light yield independent of the size of the tile. Consequently, if tower to tower PMT gain variations are normalized to the MIP signal for a tower, the calorimeter's response to localized energy deposition

anywhere (transversely and longitudinally) within it will be uniform. Because of this uniformity and relative energy calibration in terms of MIPs, all 30° pizza pan sectors can be considered to be *identical* calorimeters, *i.e.* to have identical MIP to GeV calibrations.

9.9 Test Stands

9.9.1 Test Beam Module

A mockup consisting of a 45° EM sector (three pizza pans) and a 60° hadron sector will be constructed in a manner identical to the actual device and placed permanently in the CDF test beam facility. No other test beam test will be performed on the full calorimeter. This test beam module (TBM) will be used to obtain the absolute calibration from MIPs to GeV and from wire-source response to GeV. It will also be used to study details of the performance of the full Plug Upgrade Calorimeter.

The TBM will sit on a movable stand that will allow every tower to be illuminated by a momentum-selected beam. Most of the steel absorber for the hadron calorimeter portion of the TBM is from the old 60° mockup of the gas PHA, with modification described in section 9.5.2.1 to simulate the configuration of the plug steel for Run II. The relative MIP calibration of the towers will be done with test beam muons of fixed momentum, as was done in the 1991 test beam run. The absolute calibration of the shower energy in units of MIPs to GeV will be done using momentum-analyzed electron and hadron beams of various energies. The wire-mounted source will also be used on all tiles of the TBM to verify and quantify the source technique for predicting MIP and hadron shower responses. It is expected that the source technique will permit equalizing the tower responses to within a few percent.

The relative calibration in MIP units must also be done on the actual calorimeter at B0. However, because the light yields from ionizing radiation in most scintillators increase in magnetic fields [35], the calibration at B0 must be done with the solenoidal magnetic field turned on. In principle, any increase in light yields due to magnetic field effects will produce an increased MIP response that should compensate the corresponding increase in the hadronic shower response. Thus to first order, if the absolute calibration from MIPs to GeV is obtained from the test beam

where there is no magnetic field, this absolute calibration can be transferred to B0 as long as the MIP calibration at B0 is done with the solenoid magnet on.

The magnetic field can have an additional effect: the hadron response of the CDHS iron calorimeter [36] (which is composed of magnetized steel disks in a toroidal geometry) exhibits a change of a few percent when the steel is magnetized. This is presumably due to the increased path length of curling low energy electrons in the magnetized steel. However, in the CDHS toroidal geometry only the steel was magnetized, and the scintillator was in a much lower field. In the CDF plug geometry, the magnetic field in the steel and in the scintillator is similar. The effect is therefore expected to cancel, since the fractional increased path length in the iron and scintillator will be similar.

The change in scintillator response can be monitored with the radioactive source calibration by comparing the "field on" to the "field off" response. The effect is hoped to be the same for calibrations from the source, MIPs, and hadrons. It is conceivable that the small "soft" component of the ^{137}Cs excitation of the scintillator (approximately 5% in the geometry of the hadron megatiles) contains an electronic component which could be steered away from the scintillator by the magnetic field. However, benchtop measurements with and without a few mm of plastic filter between the source tube and a tile (sufficient to remove almost all of the soft component) show no difference in the magnetic brightening curve, within an accuracy of approximately 1% or better. Consequently, it is believed that source excitation will accurately track the brightening of the calorimeter for MIPs and hadrons.

9.9.2 Cosmic Ray Test Stand

The purpose of the cosmic ray test for the complete EM calorimeter is that of obtaining a preliminary calibration to μ since the full EM calorimeter will not be tested on the test beam. The cosmic ray test stand will consist of two tracking chambers, one above and one below the calorimeter under test, and two 9.5 inch thick steel plates which will serve as a support table for the calorimeter and as an absorber for low energy cosmic rays. Figure 9.36 provides a plan view of the cosmic ray test stand.
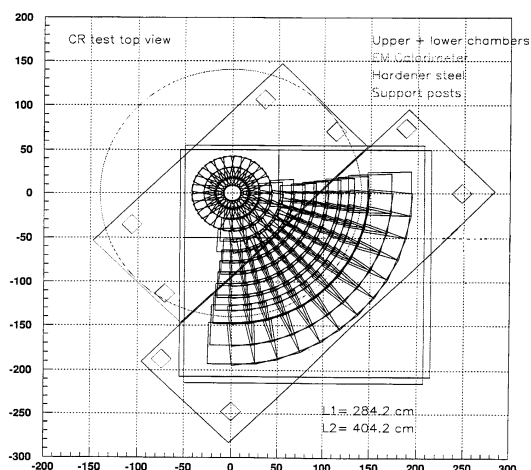
For purposes of the cosmic ray test, the calorimeter

Figure 9.36: Schematic view of the projective region covered by the tracking chambers in the cosmic ray setup.

Figure 9.37: Schematic of an engineering prototype tile-fiber assembly.

will be positioned with its axis of symmetry vertical and will rest directly on the hardener steel, which will in turn be supported approximately two feet above the floor by means of steel box-beam supports. The upper tracking chamber will be supported over the calorimeter on two parallel beams, while the lower tracking chamber will be positioned under the hardener steel. Both tracking chambers will use non-flammable gas.

The upper tracking chamber, which measures approximately 1 m$^2 \times$ 0.2 m, will be mounted on the axis of the calorimeter, 1.6 m above the front face of the calorimeter and will provide projective coverage for the entire calorimeter.

Plastic scintillator paddles above and below the upper tracking chamber will provide trigger and timing information.

The lower tracking chamber, which measures approximately 2.5 m$^2 \times$ 0.3 m, will be offset from the axis of the calorimeter as shown in Fig. 9.36 and positioned under the 9.5 in thick hardener steel on which the calorimeter rests. This chamber will provide projective coverage for one quadrant of the calorimeter.

To collect data from successive quadrants of the calorimeter, the calorimeter will be lifted by a crane and rotated by 90°. The calorimeter lifting fixture will straddle the upper tracking chamber, and will support the calorimeter by means of four cables attached to the lower calorimeter plate. The optical cables leading from the calorimeter will be disconnected prior to the rotation.
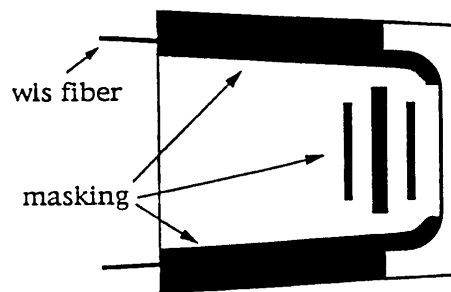
Two enclosures containing the calorimeter PMTs

will be mounted near the calorimeter, on top of the hardener steel. The optical cables leading from the calorimeter to the PMT boxes will be routed under a protective housing covering the area between the two enclosures and the calorimeter.

The DAQ for the cosmic ray test will be essentially the same as for CDF Run 1, interfaced to the DART software from the Computing Division.

9.10 Engineering Prototype Tests

9.10.1 The Engineering Prototype

A full scale engineering prototype detector was built and tested in 1991 at the Fermilab test beam facilities to investigate a number of unknown aspects of the novel technique of tile-WLS fiber calorimetry. The device consisted of EM and hadron calorimeters, and included a fine-grained shower maximum position detector using scintillating fibers.

The EM section of the prototype was composed of 48 projective towers. There were 23 sampling layers, each layer consisting of a 4.8 mm lead plate and 4 mm Bicron BC-408 scintillator tiles. The detector covered 22.5° in ϕ, and a polar angle range of $22° \leq \theta \leq 37.5°$. The 48 tiles of each layer were cut out on a Thermwood CNC milling machine at Fermilab; a U-shaped groove for the WLS fiber was made in each tile on the same machine. The tile and groove geometry is shown in Fig. 9.37. A 1 mm diameter Bicron BCF-91A WLS fiber was inserted into the groove.

Each fiber end was thermally spliced to a 1 mm diameter clear fiber. The 46 clear fibers of each projective tower were then guided along the outside of the detector to an RCA 8575 PMT.

A major goal of the construction and testing was to

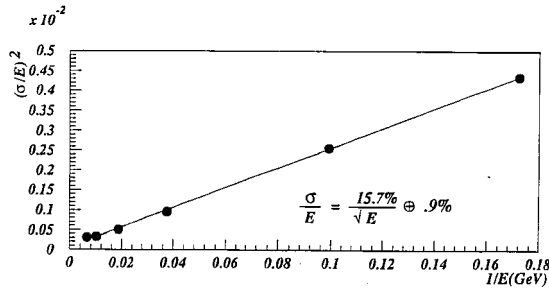$$\frac{\sigma}{E} = \frac{15.7\%}{\sqrt{E}} \oplus .9\%$$

Figure 9.38: Engineering Prototype EM energy resolution obtained from test beam electrons.

achieve uniform light response both within single tiles and from tile to tile. For single tiles the light yield varies with the position of the light generation, the highest light yield typically coming when the light is generated close to the edge of the tile. The approach taken to flatten the response was twofold; first, the position of the WLS fiber within the tile was optimized; second, the response of the high light yield areas was reduced by "masking" those areas with dark paper.

Studies of the effectiveness of both approaches were performed using a radioactive source and a scanning table. Optimal positioning of the fiber resulted in an r.m.s. variation in the light yield across EM tiles of approximately 3%. Masking reduced the r.m.s. variation to less than 2%.

To ensure that the light yield from tile to tile was as constant as possible, a large quality control effort was made in the fiber splicing and tile production processes. Source testing of the tiles showed an r.m.s. variation from tile to tile of approximately 8%. To reduce this variation further within individual projective towers, a program of longitudinal masking was developed. A radioactive source mounted on the tip of a moveable wire was passed over the surface of every tile in the calorimeter, and the peak current for every tile was recorded; this information was then used to calculate the relative light yield of each scintillator tile. Once the relative light yields of all tiles in a projective tower had been calculated, a photographic mask was produced and inserted between the optical fibers and the PMT face. The pattern on the photographic mask was generated so that the light from each tile was reduced to be equal to the light produced by the lowest light yield tile in that tower. In this way r.m.s tile to tile variations were reduced to 2-3%.

A shower maximum position detector was placed in front of the sixth layer of the EM calorimeter at a depth of 5.3 X_0. The shower maximum detector covered 15° in ϕ and a polar angle range of $22° \leq \theta \leq 37.5°$. It consisted of two layers of 2 mm diameter Kuraray SCSF38 scintillating fibers; a 15° crossing angle between the fibers of the two layers made it possible to measure particle positions. The fibers in each layer had 1 mm pitch, and there were 320 fibers per layer. The scintillating fibers were optically coupled to 1 mm diameter clear fibers through a 700 μm thick layer of Dow Corning Silgard 184. The clear fibers were routed along the outside of the EM and hadronic sections to the back of the detector, where they were read out by 8 Hamamatsu R4135A multi-anode PMTs [30]. These MAPMTs have been described in detail elsewhere [4]; but briefly, they have a crossed wire anode so that up to 228 fibers can be read out using only 36 electronic channels.

The hadronic section of the prototype was similar in design to the EM section, with the following differences: it was composed of 24 projective towers and there were 23 sampling layers, each layer consisting of a 5.0 cm steel plate and 6 mm Kuraray SCSN81 scintillator tiles. The detector covered 45° in ϕ, and a polar angle range of $14° \leq \theta \leq 37.5°$. Because of the larger tile size in the hadron section, two U-shaped grooves were cut in each tile for the WLS fibers. As in the EM section, 1 mm diameter Bicron BCF-91A WLS fibers were used, and the WLS fibers were thermally spliced to 1 mm diameter clear fibers. There were four fibers exiting from each tile, and the 92 fibers from each projective tower were routed to an RCA 8575 PMT mounted on the back of the detector.

9.10.2 Test Beam Studies

The prototype was exposed to electron, hadron, and muon beams in the CDF test beam area at MT. The response of the EM section of the calorimeter was studied to determine its energy resolution, linearity, and uniformity. The PMT gains were set to 10^5. The light yield was measured using a calibrated PMT and was found to be 400 photoelectrons (pe)/GeV, or 4.3 pe/MIP/tile. The relative tower to tower calibration was established using 100 GeV electrons. The electron beam was centered on each tower, and the energies deposited in that tower and its nearest neighbors were used to construct a 3 × 3 towers energy sum. A calibration constant was determined for each tower by iterating until the responses of all 3 × 3 tower
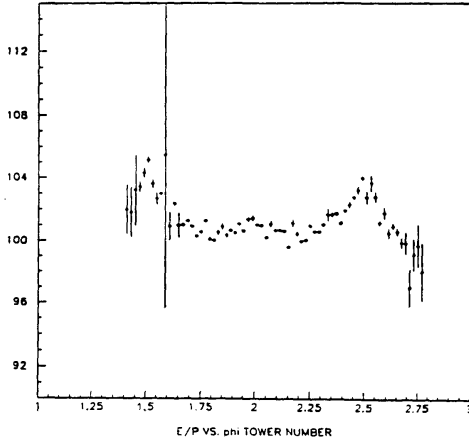
Figure 9.39: Transverse uniformity of response in an EM tower of the engineering prototype.
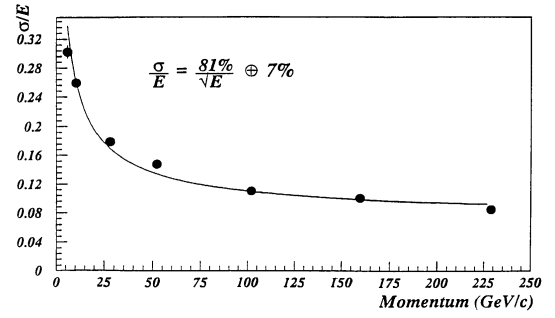

Figure 9.40: Engineering prototype hadron energy resolution obtained from test beam pions.
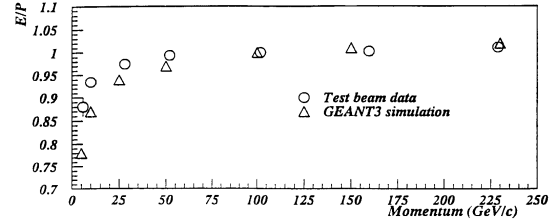
Figure 9.41: Predicted and observed response to hadrons in the engineering prototype.

sums were equal.

The device was also calibrated with high energy muons. The mean of the ratio of the electron to muon response for all towers was 1.0, with an r.m.s. variation of 4%.

The EM section energy resolution for the available electron energies is shown in Fig. 9.38 for a typical tower. Due to limitations in beam time, the energy resolution and linearity were measured for only six towers in total. The non-linearity, defined as the percent difference between the normalized response at 10 GeV and 150 GeV, corrected for leakage out the back of the EM section was typically 1%, although one tower had a non-linearity of 4%.

The transverse uniformity of the towers was also measured: using beam drift chambers to accurately determine the position of the particles, fine scans across tower faces were done with 100 GeV electrons. The results for a typical tower are shown in Fig. 9.39. The r.m.s. variation across the tower was 1.4%, consistent with the variation for single tiles measured using a radioactive source.

The energy resolution, linearity and transverse uniformity of the hadronic section were also studied. In addition, the relative response of this device to electrons and pions was studied. The hadron PMT gains were set to 5×10^5. The light yield was measured to be 39 pe/GeV, or 1.8 pe/MIP/tile. The tower to tower calibration was established by measuring the response of each tower to muons and fitting to the peaks of the resulting Landau distributions.

The energy was measured using a 3×3 tower sum,

after correcting for different relative responses. The energy resolution was measured over a range of pion energies from 5 to 230 GeV. The total energy deposited by a particle was assumed to be a linear combination of the energy in the EM and hadronic sections. A fit to the results shown in Fig. 9.40 gives an hadronic energy resolution of $81\%/\sqrt{E} \oplus 7\%$. The response of the detector, divided by the measured momentum, as a function of pion momentum, is shown in Fig. 9.41, along with the GEANT prediction. The data and GEANT prediction are normalized to the same value at a pion momentum of 100 GeV. For low energies the measured E/p is higher than the prediction.

The electron to pion response ratio (e/π) was determined by measuring the response to electrons for a hadron tower at the edge of the calorimeter that was not covered by the EM section, and comparing that response to the response to pions in a central tower. The use of different towers was dictated by the need to have lateral containment of the hadronic showers. The response for 100 GeV electrons and pions is shown in Fig. 9.42. From this data e/π at 100 GeV was measured to be $1.28 \pm 6\%$, where the large uncertainty comes from the calibration uncertainty between the two towers. A more complete de-
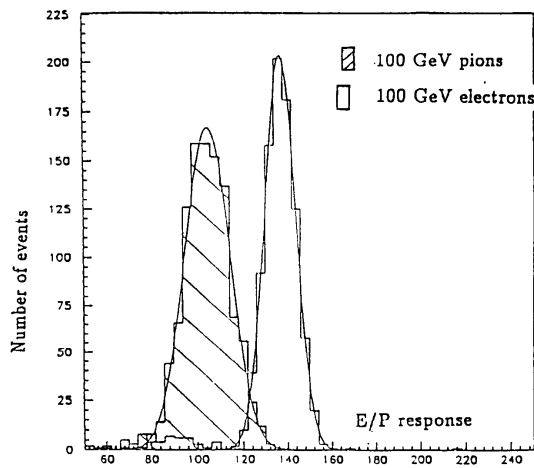
Figure 12: Response to 100 GeV electrons and hadrons.

Figure 9.42: Response to 100 GeV electrons and pions in the engineering prototype.

scription of the test beam results on the engineering prototype can be found in [8].

The shower maximum detector was designed to measure the position of electron and photon showers, and to distinguish isolated electrons and photons from $\pi°$'s. This detector and the results obtained with it in the test beam have been described elsewhere in detail [5].

9.10.3 Engineering Prototype Lessons

The device performed to expectations, but several lessons learned during the process required significant additional research and development before construction of a final calorimeter could begin. The largest problem discovered was that of routing the fiber optic readout cables to the PMTs. The readout fibers in the prototype exceeded the space limitations that exist in the real detector, and so considerable work was done to reduce the amount of fibers and to route them in a more compact manner.

In the EM and hadronic sections, the number of fibers was reduced to one per tile and the EM tile size was increased, reducing the number of towers. The scintillator fibers of the shower maximum detector were replaced by 5 mm wide scintillator strips, giving lower, but still adequate position resolution, and greatly reducing the channel count.

In addition, considerable work was done to use flat ribbon fiber cables for readout, considerably improving the packing fraction. The light output decreased when the number of readout fibers per tile was re-

duced to one, and so considerable work was done to boost the light output by mirroring the fiber end and optimizing the position of the WLS fiber in the tile.

In the end, the results from using a σ fiber pattern in the tile were uniform enough that the masking was no longer necessary. Additionally, the light output using one fiber was actually greater than had been achieved with two at the test beam. The σ pattern, with only one fiber exiting from the tile, was chosen for both the EM and the hadron detectors.

Finally, the packaging and positioning of the tiles were improved. The megatiles used in the hadron section and the scintillator rivets in the EM section were also developed in response to lessons learned in building the engineering prototype.

Bibliography

[1] The CDF Collaboration: *Proposal for an Upgraded CDF Detector* Oct 9,1990 CDF Internal Note 1172.
G.Apollinari,P.de Barbaro and M.Mishina: *CDF Calorimeter Upgrade Project*, Proc. of the 4th Int. Conf. on Calorimetry in High Energy Physics, World Scientific (1994) 200-225.

[2] F.Paige and S.D.Protopopescu, BNL Report No. 38034, 1986 (unpublished).

[3] P. Avery, K. Read, G. Trahern, Cornell Internal Note CSN-212, March 25, 1985.

[4] K.Arisaka *et al.,Position Sensitive Photomultiplier with Venetian Blind Dynodes*, UCLA internal note (1990)

[5] J. Hauser *et al.*, Nucl. Instr. and Meth. **A321**, 497-503 (1992)
Arisaka *et al.*, UCLA-HEP-90-007.

[6] G.Apollinari *et al.*, Nucl. Instr. and Meth. **A311**, 520-528 (1992).

[7] J.P.Mansour *et al.*, in Proceedings of the 1993 Scintillating Fiber Workshop, Notre Dame, IN, Nov 5-12,1993

[8] M.A. Lindgren, *The CDF Plug Calorimeter Upgrade*, in Proceedings of the Third International Conference on Calorimetry in High Energy Physics,Corpus Christi, TX, 29 Sep–2 Oct 92, eds. P.Hale and J.Siegrist, World Scientific, (1993).
J. Freeman et al., *The CDF Upgrade Calorimeter*, in Proceedings of the Second International Conference on Calorimetry in High Energy Physics, ed. A.Ereditato, World Scientific (1992), p. 189.

[9] The CDF Collaboration, "Proposal for Run II Tracking System Upgrades for CDF", CDF Internal Note 3079, March, 1995.

[10] Du Pont Tedlar-TCC15BL3, PVF film.

[11] The current candidate air conditioner is the AHP-1801HC made by Thermo Electric Cooling America Corporation (TECA).

[12] S.Kim and K.Kondo, CDF Internal Note 1788, (1991).

[13] J.Strait, CDF Internal Note 2097, (1993).

[14] T. Asakawa *et al.*, Nucl. Instrum. Methods A340(1994) 458-465.
S. Aota *et al.*, Nucl. Instrum. Methods A352(1995) 557-568.

[15] Kuraray International Corp., 200 Park Ave., New York, NY 10166.

[16] Du Pont Tyvek-1055B, spunbonded Olefin film. Mean thickness of 0.006" with 0.0025" r.m.s. spread.

[17] M.Olsson *et al.* CDF Internal Note 2582 (1994)

[18] P.deBarbaro *et al.* "CDF End Plug Hadron Calorimeter Upgrade: Design, Production and Quality Control", submitted to IEEE, Trans. Nucl.Sci. (1995)

[19] P.deBarbaro*et al.* CDF Internal Mote 2778.

[20] G.Apollinari, IEEE Trans.Nucl.Sci. Vol.40, (1993)

[21] P.Melese, "Shower Maximum Detectors Using Scintillator Strips and WLS Fibers",in Proceedings of the 1993 Scintillating Fiber Workshop, Notre Dame, IN, Nov 5-12,1993

[22] W. Koska *et al.*, "Evaluation of Candidate Photomultiplier Tubes for the CDF Plug Upgrade Calorimeter" TS-DET 95-013.

[23] W. Koska *et al.*, "Justification for Purchasing Hamamatsu R4125 Photomultiplier Tubes for the End Plug Calorimeter Upgrade Project," TS-DET 93-052.

[24] The request for quotes (JPM1270) and various addenda such as amendments to the original specifications, as well as the final purchase order, are included in TS-DET 94-034.

[25] W. Koska and S. Delchamps, "CDF Plug Calorimeter Base Design Considerations," TS-DET 93-058.

[26] I. Fiori *et al.*, "Gain and Dark Current versus Voltage Measurements on Hamamatsu and Philips Photomultiplier Tubes" TS-DET 92-001. W. Koska and I. Fiori, "Gain vs. Voltage and Pulse Height Resolution Measurements for the First Twenty Production PMT's" TS-DET 93-072.

[27] Q. Shen, "Linearity of the 19 mm Hamamatsu R4125 Photomultiplier Tubes," TS-DET 93-016.

[28] G. Comby and R. Meunier, Nucl. Instr. and Meth. **A269**, 246 (1988); F. Takasaki *et al.*, Nucl. Instr. and Meth. **A260**, 447 (1987); M. Salomon and S.S.A. Williams, Nucl. Instr. and Meth. **A241**, 210 (1985); and J. Ditta *et al.*, Nucl. Instr. and Meth. **220**, 343 (1984).

[29] P. Cushman and S. Hou, Nucl. Instr. and Meth. **A339**, 456 (1994)
J. Bahr *et al.*, Nucl. Instr. and Meth. **A330**, 103 (1993)
G. Apollinari *et al.*, Nucl. Instr. and Meth. **A324**, 475 (1993).

[30] Hamamatsu Photonics K.K., Electron Tube Center 314-5, Shimokanzo, Toyooka Village, Iwata-gun, Shizuoka-ken, Japan.

[31] S1722-02- type PIN by Hamamatsu Corp., Bridgewater, NJ.

[32] R.L. Heath *et al.*, Nucl. Instr. and Methods, 162 (1979) 431-476.

[33] P. Auchincloss et al., Nucl. Inst. & Methods **A343**, 463 (1994)

[34] A. Beretras et al., Nucl. Inst. & Methods **A329**, 50, (1993)

[35] J.Mainusch et al., Nucl. Instr. and Methods, **A312** (1992) 451
D.Blömker et al., Nucl. Instr. and Methods, **A311** (1992) 505.

[36] H.Abramowicz et al. (CDHS) Nucl. Instr. and Methods, **180** (1981) 429.

[37] K. Hara *et al.*, Nucl. Instrum. and Methods A348 (1994) 139-146.

[38] S. Aota *et al.*, Nucl. Instrum. and Methods A357 (1995) 71-77.

[39] S. Aota *et al.*, CDF Internal Note 3141 (1995)

[40] K. Hara, CDF Internal Note 2958 (1995)

[41] CAEN SpA , e-mail INFO@CAEN.IT, URL: http://www.caen.it, Via Vetraia, 11 I-50049 Viareggio,(Italy)